Pin4 Links Post-transcriptional and Transcriptional Responses to Glucose Starvation in Yeast

Michaela Ristová[1], Katherine Bexley[1], Vadim Shchepachev[1], Atlanta G. Cook[1], David Tollervey[1,2]

1 Wellcome Centre for Cell Biology, University of Edinburgh, Edinburgh, UK

Michaela Ristová: s1507601@ed.ac.uk

Katherine Bexley: s2247997@ed.ac.uk

Vadim Shchepachev: v.shchepachev@gmail.com

Atlanta G. Cook: atlanta.cook@ed.ac.uk

David Tollervey: d.tollervey@ed.ac.uk

2 Lead contact

ABSTRACT

Adaptation to environmental change is essential in all organisms, with RNA-binding proteins (RBPs) playing critical roles in rapid cellular responses. We analyzed the largely uncharacterized yeast RBP Pin4, and its involvement in adaptation to glucose depletion. A UV crosslinking technique to identify protein-RNA interactions (reCRAC) revealed that in glucose conditions Pin4 selectively binds a specific motif in 3' UTRs of mRNAs involved in glycolysis, amino acid, and mitochondrial metabolism. Following glucose withdrawal, Pin4-RNA binding was greatly reduced, with residual binding favoring transcripts associated with protein translation. Cells lacking Pin4 were greatly impaired in recovery from nutrient starvation and hypersensitive to oxidative stress, consistent with the mRNA targets. RNAseq and reporter assays indicated that loss of Pin4 caused increased target mRNA abundance. In wildtype yeast, glucose depletion induces “diauxic shift”, with massive changes in transcription patterns. Very unexpectedly, this response was almost entirely abolished in cells lacking Pin4, or carrying a point mutation in its RNA-recognition motif. We conclude that Pin4 contributes to energy homeostasis by regulating post-transcriptional and transcriptional responses, and postulate that this key stress response pathway is riboregulated.

INTRODUCTION

The capacity to adapt to ever-changing environments is a fundamental trait necessary for the survival of all living organisms. This adaptability encompasses specific responses to a wide range of stressors such as nutrient depletion, temperature fluctuations, and pH changes [1]. Central to these adaptive responses are RNA-binding proteins (RBPs), which regulate a multitude of critical steps throughout gene expression [2,3].

The budding yeast *Saccharomyces cerevisiae* grows on plant surfaces and is exposed to many environmental insults. For example, a rain shower will result in immediate nutrient deprivation, perhaps only transiently. Yeast has long been used as a model eukaryote, to study responses to a multitude of stressors. Notable among these stress responses is the diauxic shift, the metabolic switch induced by glucose depletion, which drastically affects yeast cell physiology and behavior [4]. Under glucose abundant conditions, yeast cells metabolize glucose in preference to any other available carbon sources, utilizing aerobic fermentation. Glycolysis converts the glucose to CO_2 and ethanol, which are excreted despite the availability of oxygen. This metabolic preference for aerobic fermentation – termed the Crabtree effect – has been observed across diverse biological systems, including plant pollen, Trypanosomatids, skeletal muscles, and tumor cells, where it is referred to as the Warburg effect [5–8]. The predominant hypothesis for the emergence of the Crabtree effect centers on the rapid production of ATP and the evolutionary advantage of quickly producing progeny [9]. Following glucose depletion, the switch from fermentation to respiration involves a two-stage response: a rapid post-transcriptional response, followed by a slower transcriptional response. The initial post-transcriptional response primarily affects protein synthesis, followed by alterations in mRNA splicing, polyadenylation, RNA stability, RNA modifications, spatial localization, and condensate formation [10–14]. The subsequent transcriptional response unfolds over several minutes, with upregulation of specific stress-response genes and suppression of those involved in ribosome biogenesis and growth. Central to the regulation of this response are three major signaling pathways associated with yeast glucose metabolism: the Snf1, PKA, and Snf3/Rgt2 pathways [15–18].

Supporting RNA binding proteins as central to rapid adaptive responses, a recent study identified extensive remodeling of the yeast RNA-protein interactome in response to glucose withdrawal or heat shock within a 16 min timeframe [19]. Key factors in protein synthesis were notably affected, consistent with the widespread shutdown of translation during stress. Intriguingly, among the most strongly altered RBPs, several were largely uncharacterized, notably Pin4, Mrn1, Pbp2 and Nab6. Subsequent investigations implicated Mrn1 and Nab6

in a novel post-transcriptional cell wall integrity pathway [20]. Here, we characterize the role of Pin4 in the cellular response to glucose withdrawal.

Previous screens identified Pin4 as a protein that alters yeast prion formation and as a Rad53 interactor, implicated in the responses to methylmethane sulfonate (MMS) and bleomycin treatment, and normal G2/M cell cycle progression [21–23]. However, these putative functions were not clearly related to RNA interactions, so we sought to investigate these in detail. We conclude that Pin4 has a pivotal role in yeast energy metabolism, regulating both post-transcriptional and transcriptional adaptations to cellular stress induced by glucose depletion. Identifying the function of this critical protein highlights the potential for a class of previously unidentified RNA binding proteins that connect external signaling to a regulatory RNA interaction network.

RESULTS

Pin4 has a non-canonical RRM and large unstructured regions

Since very little functional information was available for Pin4, we first sought structural features that might point to its role in the cell. Conserved domains were analyzed utilizing multiple sequence alignments from the NCBI Conserved Domain Database [24]. Pin4 is 668 amino acids in length, with an unstructured Q/N-rich C-terminal region previously identified as a prion-forming domain [23,25,26]. Database searches and AlphaFold3 predicted three further domains: an RNA Recognition Motif (RRM), a coiled-coil (CC) domain, and an R3H domain with all other parts being largely unstructured (Fig. 1A) [24,27].

The Pin4 RRM is from the family “RRM_PIN4_like” domain (Fig. 1A) [24], which is also present in five annotated proteins from fungal species and one protozoan (Supp. Figs. 1A and 1B). Of these, only *Schizosaccharomyces pombe* Cip1 and Cip2 are characterized, and were reported to function in gene regulation during oxidative stress [28]. Interestingly, the Pin4 RRM differs from canonical RRM domains, with alterations in the characteristic ribonucleoprotein (RNP) motifs. Positions 3 and 5 in RNP-1 and position 2 in RNP-2 are typically aromatic residues, Phe or Tyr, important for RNA binding. In Pin4, the corresponding amino acids are Leu128 (RNP-1 position 3), Phe130 (RNP-1 position 5), and Val 88 (RPN-2 position 2) (Supp. Figs. 2A and 2B). Although, the leucine and valine residues are not aromatic, but hydrophobic, it is not completely unusual as equivalent residues can be also found in the same positions in RRMs of other yeast RNA binding proteins, including UPF3 and TAP [29].

The Pin4 R3H is from the family of “R3H_RRM” domain, identified in other ten fungal proteins, mostly uncharacterized except for *S.pombe* Cip2 (Supp. Figs. 1A and 1B). R3H

domains can dimerize [30,31] and AlphaFold3 reproducibly modeled the R3H domain of Pin4 as a homodimer, with good supporting statistics (Supp. Fig. 2C). This suggests that the R3H domain of Pin4 may be a dimerization element rather than a nucleic acid binding domain. The CC domain is predicted to mediate protein interactions, and also lies close to the RRM (Supp. Fig. 2D) [32], indicating a scaffolding role that could facilitate spatial proximity between RNA targets and protein interactors.

Pin4 predominantly binds mRNA 3' untranslated regions

Pin4 was an outlier in the total RNA-bound proteome following stress [19]. We therefore identified RNAs bound by Pin4 during growth in 2% glucose medium and following transfer to 2% glycerol plus ethanol (Gly/EtOH) medium for 16 min, to induce diauxic shift. To allow purification, we expressed Pin4 as a fusion protein with an N-terminal tandem-affinity tag containing a single FLAG epitope-Ala_4-His_8 (FH tag) [19]. The 20 amino acid FH tag was introduced into the chromosomal *PIN4* gene under control of the endogenous promoter, using CRISPR-Cas9 without a selective marker [33]. FH-Pin4 is the only form of Pin4 in these cells, which showed no clear growth defects.

We initially applied the published protocol for crosslinking and analysis of cDNA (CRAC) [34]. However, Pin4 underwent substantial degradation during purification (Supp. Fig. 3A). We therefore developed a modified protocol, termed reverse CRAC (reCRAC) [35], which notably enhanced the integrity of Pin4 (Fig. 1B, Supp. Fig. 3A). In reCRAC, the tandem affinity purifications steps are reversed relative to CRAC. Briefly, cells are lysed in highly denaturing buffer, including 6M Guanidine-HCl, to immediately inactivate cellular proteases. FH-Pin4 was recovered on Ni-NTA beads in denaturing buffer. While still immobilized on the Ni-NTA beads, but under non-denaturing conditions, bound RNAs were subjected to partial Benzonase digestion, the 5' ends were labeled with $^{[32]}P$, and linkers were added to the termini. Protein-RNA complexes were eluted and further purified on an anti-FLAG column. Following elution, complexes were gel purified using the labeled RNA as marker, and the proteins were degraded with proteinase K. RNA was recovered and used for RT-PCR amplification and sequencing. Replicate experiments showed good reproducibility (Supp. Figs. 3B and 3C).

During reCRAC, samples were barcoded and mixed prior to RT-PCR amplification. In consequence, relative numbers of total reads recovered for each condition approximates to overall crosslinking efficiency. The total number of reads in the FH-Pin4 libraries decreased dramatically following glucose withdrawal, indicating strongly decreased overall RNA binding (Fig. 1C). In glucose rich conditions, Pin4 predominantly targeted mRNAs, which constituted

about 70% of its interactions (Fig. 1D). Reads were also mapped to “non-coding” RNAs, but these were distributed over a large and heterogeneous set of RNAs, mainly antisense and intergenic, and specific interactions were not evident. Following glucose depletion, there was a 50% reduction in the fraction of reads mapped to mRNA (Fig. 1D). Absolute recovery of rRNA was similar to the untagged control, indicating that these represent non-specific interactions (Supp. Fig. 3D), and the apparent increase following glucose depletion likely reflects loss of mRNA binding.

To assess Pin4 binding specificity, we analyzed the distribution of FH-Pin4 bound sequencing reads across the 5’ untranslated region (UTR), coding sequence (CDS), and 3’ UTR of all annotated mRNAs. In the presence of glucose, Pin4 predominantly bound 3’ UTR regions; these formed 78% of reCRAC reads compared to 12% in total RNA from the RNAseq control (Fig. 2A). This pattern of predominant 3’ UTR binding is apparent in a metagene plot in which reCRAC reads are mapped onto mRNAs aligned at their 3’ ends, revealing a distinct 3’ peak (Fig. 2B). On individual mRNAs with strong Pin4 binding relative to RNAseq, the prominent peak in the 3’ UTR is very clearly visible (shown for *TPI1*, *ILV5*, *GPM1* and *RPS12* in Fig. 1C).

Following glucose withdrawal, the enrichment for Pin4 binding to 3’ UTRs is notably decreased (49% of all reads) (Fig. 2A), although some indication of preferential 3’ binding remained (Fig. 2B). On most top mRNAs, residual Pin4 association remained enriched on the 3’ UTR (Fig. 2C). However, a subset had substantial CDS binding after glucose depletion. These transcripts were generally related to ribosomes and translation (Supp. Fig. 3E; Supp. Table 4). As an example, *RPS12* (Fig. 2C) has substantial Pin4 binding in the CDS, even though the highest peak was still in the 3’ UTR.

A binding motif for Pin4

In reCRAC, the direct sites of RNA-protein crosslinks can be pinpointed by searching for deletions within recovered sequences. At the end of the experimental procedure, the bound protein is degraded by proteinase K treatment, leaving at least one amino acid on the RNA. Due to this, reverse transcriptase can skip the crosslinked nucleotide. Nucleotide substitutions can arise from other causes (PCR, RT, sequencing) but single nucleotide deletions are characteristic, and otherwise very rare. Using this data on Pin4 binding sites to identify potential sequence determinants, we focused on high-confidence Pin4 targets under both glucose and Gly/EtOH conditions; the cut off being at least 0.3% of the library in at least two replicates (35 transcripts in glucose; 38 transcripts following withdrawal) (Supp. Table 5). After identifying the most significant deletion peaks within these transcripts, we ran MEME

analysis on the flanking 20 nucleotide sequences. We discovered a consistent T(A/T)ATG(A/T) motif across both conditions (Fig. 2D). This motif was generally located either precisely at the peak of binding (Fig. 2E), or immediately adjacent to the highest deletion peak (Supp. Fig. 3F). The close association of the motif with the peak of Pin4 binding was maintained in glucose replete and depleted conditions.

Analysis of the high-confidence Pin4 targets showed no consistent pattern of pairs of binding sites that would indicate binding as a homodimer. Analysis of mRNAs that were well bound by Pin4, but not enriched relative to mRNA abundance (on or below the diagonal in Figs. 3A and 3B), showed no clear motif enrichment.

We conclude that the T(A/T)ATG(A/T) motif is very likely to represent a direct Pin4 recognition element.

Pin4 selectively binds metabolic and growth-associated transcripts

To assess mRNA target specificity, Pin4-associated RNAs isolated with reCRAC were compared to mRNA abundances from WT RNAseq (Supp. Table 6; Figs. 3A and 3B). It showed that majority of mRNAs associate with Pin4: confident strongly bound targets that showed enrichment are highlighted. In glucose medium, the most enriched Pin4-associated transcripts were predominantly involved in metabolic and pro-growth pathways (Fig. 3A). Key glycolytic enzymes emerged as top targets in both conditions, including *TPI1* (triose phosphate isomerase), *ADH1* (alcohol dehydrogenase), and *GPM1* (phosphoglycerate mutase) (Fig. 3C). *TPI1* alone represented about 4% of reads, versus 0.5% from RNAseq in glucose (Fig. 3D). Transcripts involved in mitochondrial function (e.g., *ILV5*) and amino acid metabolism (e.g., *HIS4*) were strongly targeted only in glucose-rich conditions.

For high confidence interactions (≥0.3% of library in ≥ 2 replicates) (Supp. Table 5) comparing Pin4 binding relative to transcript abundance confirmed significant GO term enrichment: glycolysis ($p=0.0288$), amino acid metabolism ($p=0.0079$), and mitochondrial metabolism ($p<0.0001$) (Fig. 3E). This enrichment was also reproduced by grouping the transcripts based on their binding enrichment and GO term analysis using the Proteomaps tool [36] (Supp. Fig. 4A). These high-confidence targets showed good reproducibility across replicates in both conditions (Supp. Fig. 4B).

Following glucose withdrawal, there were fewer clearly enriched targets, consistent with the metagene plot, but some of the same genes remained enriched, including the glycolytic enzymes. Representation was strongly increased for several translation-related transcripts

(Fig. 3F), which correspond to the mRNAs showing Pin4 association across the CDS (e.g. *RPS12*) (Fig. 2C; Supp. Fig. 2E).

Pin4-deficient cells are sensitive to glucose depletion and mitochondrial stress

As Pin4 binds mRNAs connected to central carbon metabolism and mitochondria, we tested for growth phenotypes after precisely deleting *PIN4* using a KanMX6 cassette [37]. In glucose medium, *pin4Δ* strains showed only a slight increase in doubling time compared to WT (Supp. Fig. 5A). However, upon shifting to 2% Gly/EtOH medium, *pin4Δ* cells exhibited greatly increased lag before reinitiation of growth (Supp Fig. 5B), followed by a steady-state doubling time of approximately 7 hr versus 6 hr for the WT (Supp. Fig. 5C). Under oxidative stress induced by 0.5 mM hydrogen peroxide, *pin4Δ* cells had a lag phase of 30 hr compared to 15 hr for WT (Supp. Figs. 5D and 5E). At 1 mM H_2O_2, *pin4Δ* cells showed no growth, whereas WT cells remained viable. Exposure to glyoxal, which collapses mitochondrial membrane potential, also led to slowed growth and increased lag phase in *pin4Δ* cells (Supp. Fig. 5F), with growth progressively decreasing at higher concentrations compared to WT (Supp. Fig 5G).

We conclude that cells lacking Pin4 exhibit hypersensitivity to glucose withdrawal or mitochondrial stress, consistent with the targets for Pin4 binding.

Pin4 negatively regulates target mRNA abundance

To determine whether the loss of Pin4 affects target mRNA abundance, we performed RNA sequencing on WT and *pin4Δ* cells in glucose medium. Differential expression (DE) analysis identified 58 mRNAs showing the most altered expression between the WT and *pin4Δ* (fold change ≥ 2.0; adj. $p \leq 0.05$) (Fig. 4A; Supp. Table 7). The most upregulated mRNAs were enriched for cell wall components (Supp. Fig. 6A), but these generally had very low expression, making the significance unclear. Downregulated genes were preferentially linked to transmembrane transport and vitamin binding (Supp. Fig. 6B). The mRNA showing strongest DE were not top Pin4 targets. However, comparison of Pin4 mRNA binding and changes in abundance in *pin4Δ* cells revealed generally increased abundance for preferential Pin4 targets (high confidence mRNA targets with at least 0.3% of the library) (Fig. 4B).

Analysis of recent proteomic data for *pin4Δ*, based on a genome-wide deletion screen, also showed modestly increased protein abundances for the products of high-confidence Pin4

mRNA targets [38]. This suggested that Pin4 binding might destabilize target mRNAs and/or inhibit translation.

To test this hypothesis, we used the MoClo system to generate reporter constructs (Fig. 4C). These express the Venus fluorescent protein under the control of the *TEF2* promoter (P_{TEF2}), which is characterized by high and stable expression levels in both glucose and Gly/EtOH media, with expression unaffected in *pin4Δ* cells. We incorporated the 3' UTR and terminator sequences of two strong Pin4 targets, *TPI1* (T_{TPI1}) and *GPM1* (T_{GPM1}), extending 479 and 500 nucleotides, respectively, beyond the stop codons. As a control, we used the 3' UTR and terminator sequence of *PNC1* (T_{PNC1}; 379 nucleotides), which is not bound by Pin4. The constructs where chromosomally integrated into the yeast HO locus, and Venus expression was monitored for mRNA (RT-qPCR) and protein (western blot levels).

In strains lacking Pin4, reporter constructs containing *TPI1* and *GPM1* 3' UTRs showed a mild increase in mRNA levels in both glucose and following transfer to Gly/EtOH (16 min), which was not observed with the *PNC1* control (Fig. 4D). This result was consistent with our RNAseq data (Fig. 4E). Western blot analysis mirrored these findings at the protein level, displaying a modest increase in the expression of reporters with *TPI1* and *GPM1* 3' UTRs in *pin4Δ* cells in both nutritional states (Fig. 4D; Supp Fig. 6C). Although the increases observed by RT-qPCR failed to pass a rigorous test for statistically significance, the trend of upregulation among Pin4 targets was seen across all analyses; PCR and western on reporters; RNAseq and proteomics on endogenous mRNAs and proteins. Together, these data support the conclusion that Pin4 binding modestly destabilizes target mRNAs, with consequent reductions in protein abundance.

Impaired transcriptional response to stress in Pin4-deficient cells

Several mRNAs with altered abundance in *pin4Δ* cells were not strongly bound Pin4 targets (Fig. 4F). This indicated that the role of Pin4 involves mechanisms beyond specific interactions with individual mRNA. Wild-type cells undergo profound transcriptional changes following glucose withdrawal, characterized as the integrated stress response (ISR), which alters the abundance of several hundred mRNAs to promote cellular recovery. We analyzed RNA sequencing data following glucose depletion to determine whether the loss of Pin4 affects this response.

Principal component analysis (PCA) revealed surprisingly distinctive patterns: WT replicates clustered well in each condition and were clearly separated between glucose replete and

glucose depleted conditions. In striking contrast, *pin4Δ* samples clustered together regardless of the treatment (Fig. 5A). This clustering suggested minimal transcriptional changes in *pin4Δ* cells following glucose depletion. Spearman correlation heatmaps confirmed the distinction between WT in glucose versus Gly/EtOH, but high similarities in both conditions for *pin4Δ* cells – as well as consistency in the replicates (Fig. 5B). A heatmap of gene expression (Fig. 5C) further confirmed the minimal variation in *pin4Δ* cells following glucose depletion. This indicates a critical role for Pin4 in the transcriptional response to glucose starvation.

Detailed analysis of all individual transcripts further underscored these observations. Following glucose depletion, differential gene expression (DE) analysis identified 645 transcripts present at significantly different levels in WT and *pin4*Δ cells (fold change ≥ 2.0; adj. $p \leq 0.05$), a strikingly large number (Fig. 5D; Supp. Table 8). In almost all cases, DE reflects stress-induced changes, up and down, in the WT that are lost in the *pin4*Δ. As expected, stress response genes were strongly upregulated in the WT, whereas pro-growth genes were downregulated, including RNP and ribosome biogenesis. In cells lacking Pin4, the latter were little altered and thus elevated in comparison to the WT (Fig. 5E; Supp. Fig. 7A). Additionally, mRNAs linked to catabolic and respiration-related processes were lower in *pin4*Δ (Fig. 5F; Supp. Fig. 7B).

Pin4 domains required for the transcriptional response to glucose starvation

To better characterize the role of Pin4 in the transcriptional response to glucose starvation, we constructed Pin4 mutant strains lacking functional domains.

To assess the role of RNA binding, we created strains precisely lacking the RRM domain ($pin4_{RRM\Delta}$) or with point mutations ($pin4_{RRM\text{-}M1}$: V88A, L128A, F130A) predicted to disrupt RNA binding while maintaining RRM domain structure (Fig. 6A). Unexpectedly, the $pin4_{RRM\text{-}M1}$ variant exhibited notably slower growth than WT, *pin4Δ* or $pin4_{RRM\Delta}$ strains (Supp. Fig. 7C). The basis for this is unclear and currently under investigation.

The effects of these mutations were tested by RT-qPCR on the *MTH1*, *HSP12*, and *HXT7* genes, which were strongly upregulated following glucose withdrawal in the WT. Expression was analyzed during growth on glucose, and 16 or 32 min after transfer to Gly/EtOH medium. In glucose medium, the mRNAs were expressed at similar, very low levels in all strains, WT, *pin4*Δ, $pin4_{RRM\Delta}$ or $pin4_{RRM\text{-}M1}$. Following glucose depletion, the mRNAs were strongly induced in the WT, but this was much less marked in *pin4*Δ or $pin4_{RRM\Delta}$ (Fig. 6B). In

the *pin4*$_{RRM\text{-}M1}$ strain induction of *HSP12* was reduced to a similar extent to *pin4*Δ, while induction of *HXT7* and *MTH1* was even lower in *pin4*$_{RRM\text{-}M1}$.

The Pin4 C-terminal region is intrinsically disordered and potentially prion-forming [39–41], but includes the R3H domain. To test its function, we created a construct truncated after the N-terminal 200 aa (*pin4*$_{\Delta CT}$), fused with GFP to improve stability (Fig. 6A). Following transfer of *pin4*$_{\Delta CT}$ to Gly/EtOH for 16 min, transcriptional induction of *MTH1*, *HSP12*, and *HXT7* was significantly reduced relative to the WT, and very similar to *pin4Δ* and *pin4*$_{RRM\Delta}$ (Fig. 6C).

We conclude that both a functional RRM domain and the disordered C-terminal region of Pin4 are required for the transcriptional response to glucose withdrawal, suggesting functional interactions with both RNA and proteins.

Role of Pin4 in bridging post-transcriptional and transcriptional stress responses

To place Pin4 function in the wider context of stress responses we assessed immediate post-transcriptional effects. A very rapid reduction in global protein synthesis normally follows glucose depletion [14,19]. Polysome analyses indicated a comparable loss of translation in WT and *pin4*Δ cells (Supp. Fig. 7D) following transfer from glucose to Gly/EtOH medium, suggesting that this initial response to glucose starvation is unperturbed.

In WT yeast, glucose depletion induces formation of Hsp104 granules, an HSP100-family disaggregase that resolves stress-induced protein aggregates [42]. In live cell imaging of WT cells (Fig. 7A), 18% of cells had at least one Hsp104 granule on glucose medium, rising to almost 40% during the first 24 min following transfer to Gly/EtOH medium. Granule frequency plateaued around 70% after 90 min (Fig. 8B), as reported [43]. In contrast, *pin4*$_{RRM\Delta}$ showed a significantly reduced response. The percentage of cells exhibiting at least one Hsp104 granule increased only mildly, from approximately 20% in glucose to a plateau of around 30%, after 45 min in Gly/EtOH medium (Fig. 8C). This muted response was also seen for total Hsp104-GFP induction (Fig. 8C).

We conclude that Pin4 is dispensable for the rapid, initial shutdown of protein synthesis following starvation, but required for subsequent post-transcriptional, and longer term, transcriptional responses.

DISCUSSION

RNA binding proteins (RBPs) play crucial roles in cellular responses to many environmental stresses. We previously screened for global changes in the RNA-protein interactome on a short timescale following a variety of stresses, including heat shock and glucose withdrawal [19]. Unexpectedly, a set of largely uncharacterized proteins were among the most stress responsive RBPs. Included in these “unknome” factors was Pin4, which we functionally characterized here.

Using the newly developed reCRAC technique,[35] Pin4 showed a distinctive pattern of binding to mRNA 3’ UTRs during growth on glucose medium. The mRNAs with strong Pin4 binding, relative to RNA abundance, all carried a clear consensus motif. This was located close to the site of crosslinking, which can be identified at the nucleotide level in reCRAC, strongly supporting its role as a direct Pin4 recognition element. However, 3’ UTRs of almost all mRNA were detectably bound by Pin4, indicating that recognition by Pin4 has at least two components: Recognition of some feature(s) common to all mRNA 3’ UTRs, plus binding to a specific sequence motif. Notably, the functional classes of mRNAs favored for Pin4 binding were not random. They included most glycolytic enzymes, plus several key mitochondrial proteins and a small number of important enzymes in amino acid metabolism.

Following glucose depletion, overall RNA crosslinking of Pin4 was substantially reduced, particularly for mRNAs. However, the preference for 3’ UTR binding and the same enriched motif were preserved, suggesting that the recruitment mechanism is retained. The reduced interactions could reflect altered Pin4 affinity, e.g. due to phosphorylation, which is altered at multiple sites in response to stress [44–49], or reductions in the availability of Pin4 and/or mRNAs. mRNA availability might be reduced by sequestration into cytoplasmic condensates [50,51]. Pin4 homodimerization through the R3H domain might reduce its availability, but there was no indication of binding RNA as a dimer in our data. Potentially, Pin4 may form aggregates via its prion-like domain, affecting its interactions with RNA [23,25,26]. We noted that translation-related transcripts showed increased Pin4-binding following glucose withdrawal. This included binding throughout CDS, where we were unable to detect a Pin4-motif. Following glucose withdrawal, these pre-stress mRNAs are still present in large quantities but are largely ribosome-free [52]. We hypothesize that the CDS signal reflects Pin4 association/close proximity in the absence of sequence-specific binding, potentially within cytoplasmic condensates [50,51].

Analyses using reporter constructs indicated that Pin4 binding modestly destabilized mRNA targets, under both glucose-replete and glucose-depleted conditions, with consequent

reductions in reporter protein accumulation. This conclusion was supported by RNA sequencing in strains lacking Pin4, and a recent, systematic analyses of protein abundances in yeast deletion mutants [53]. Previous high-throughput analyses reported protein-protein interactions between Pin4 and components of the CCR4-NOT complex (Caf40, Cdc39, Cdc36, Mot2, Ccr4), which mediates mRNA degradation [54–56]. The localization of Pin4 binding sites within the 3' UTR would be consistent with destabilization of mRNA targets. The retargeting of Pin4 onto the non-ribosome bound, translation-related transcripts following stress might also fit this model. The preferred mRNA targets for Pin4 in glycolysis and mitochondria suggested roles in energy metabolism. In glucose medium, *pin4Δ* cells exhibited hypersensitivity to both H_2O_2, which induces oxidative stress, and glyoxal, a reactive carbonyl species that generates reactive oxygen species and disrupts mitochondrial membrane potential [57]. We speculate that this hypersensitivity is linked to misregulated mitochondrial function due to imbalances in protein production in the absence of Pin4.

Unexpectedly, loss of Pin4 profoundly affected transcriptional adaptation to glucose depletion, almost completely abolishing the induction of stress-responsive mRNAs. We identified 645 mRNAs that were significantly differentially expressed between Pin4-deficient cells and WT cells following starvation. In the WT, mRNAs related to stress response, mitochondria, and respiration were massively upregulated, consistent with the shift from fermentation to respiration. In cells lacking Pin4, these changes were absent, and the transcriptional profile closely resembled glucose-rich conditions. The cells apparently failed to recognize or respond to the stress applied. Given this lack of transcriptional response, it is unsurprising that *pin4Δ* cells displayed greatly impaired recovery of growth following transfer from glucose to non-fermentable carbon sources. However, the exact point at which Pin4 operates within the glucose signaling pathways, and how its absence blocks the transcriptional response, remains unclear. Previous data suggest links between glycolytic flux and signaling of the presence or absence of glucose [18] and Pin4 might function here.

To test whether RNA binding by Pin4 is needed for the transcriptional response, we generated strains lacking the single RRM of Pin4 or carrying RRM point mutations predicted to disrupt protein-RNA binding but not domain structure. Both mutants recapitulated the *pin4Δ* transcription phenotype in response to glucose withdrawal. This strongly indicates that RNA binding of Pin4 is integral to induction of the transcriptional stress response. It could be envisaged that Pin4 has two binding modes – specific binding of particular mRNA targets with biological roles and a "bulk" RNA binding that is non-specific. Major Pin4 target mRNAs did not include key glucose signaling factors or other obvious transcriptional regulators. Moreover, the modest post-transcriptional destabilization of target mRNAs contrasts with the

massive loss of transcriptional changes observed in cells lacking Pin4. We would therefore suspect that this “bulk” binding may relate to the transcriptional effects of Pin4 that extend beyond its targets. This suggests that alterations in total RNA interactions might regulate Pin4 function.

Deletion of C-terminal region in *pin4*$_{\Delta CT}$ also blocked transcriptional reprograming. The region deleted was previously reported to form prion-like aggregates [23], suggesting that this may be the key missing function in these mutants. However, initial live cell imaging did not reveal clear Pin4 aggregation. The deletion also removes a putative R3H domain, which modelling suggested would support homodimerization. However, the reCRAC data provided no evidence that the RNA-bound form of Pin4 is a homodimer. It is possible that the release of Pin4 from mRNA may allow Pin4 to interact with other factors, and loss of this interaction may contribute to the absence of a transcriptional stress response.

To further address the stress responses in the absence of Pin4, or its RRM, we quantified Hsp104 granules, which form in response to protein misfolding following environmental insults [58]. Live cell imaging revealed that *pin4*$_{RRM\Delta}$ cells almost entirely failed to induce Hsp104 granule formation, highlighting the loss of stress response.

In summary, we propose a dual-function model for Pin4 in glucose-rich and glucose-depleted conditions (Fig. 8). In glucose conditions, Pin4 binds to the 3’ UTRs of metabolic and pro-growth mRNAs, and regulates gene expression post-transcriptionally by promoting their destabilization. Following glucose withdrawal, Pin4 s required to activate the transcriptional starvation response through mechanisms involving its RNA recognition motif and prion-forming domain. The requirement for RRM function suggests that regulation requires RNA interactions, and represents an example of riboregulation.

Glucose signaling pathways have previously been extensively characterized, without identification of a role for Pin4. However, these were based on genetic screens on the timescale of days, whereas we assessed responses over minutes. We note that this is the timescale needed for rapid and reversible responses to environmental stimuli. Loss and restoration of nutrient availability on plant surfaces might occur several times a day, and transient but substantial stresses will be the norm in many biological systems. Post-transcriptional mechanisms likely provide the first responses, on second to minute timescales, followed by longer term transcriptional changes that persist for days. It might be beneficial to have mechanisms that bridge and coordinate these different levels of response, and we predict that Pin4 plays such a role.

MATERIALS AND METHODS

Reagents

10 mM dNTP mix (Thermo Scientific, Cat#18427013)

10x NEBuffer 2.1 (NEB, Cat#B7202)

10x T4 DNA ligase buffer (NEB, Cat# B0202S)

5-alpha Competent E.coli High Efficiency (NEB, Cat# C2987I)

Act1 primary antibody (Abcam, Cat# 8224)

BamHI-HF (NEB, Cat# R3136S)

BclI (NEB, Cat#R0160S)

BsaI-HF-v2 (NEB, Cat# R3733S)

BsmBI-v2 (NEB, Cat# R0739S)

Concanavalin A (Sigma, Cat# C2272-2MG)

CSM Complete (Formedium, Cat#DCS0011)

CSM Single Drop-out -Trp (Formedium, Cat#DCS0149)

Cycloheximide – stock of 20 mg/ ml in EtOH prepared and stored at -20C (Sigma-Aldrich, Cat#C7698-5G)

D (+) – Glucose Anhydrous (Thermo Scientific, Cat#10141520)

DNase/RNase free water

EcoRI-HF (NEB, Cat# R3101S)

EDTA-free cOmplete protease inhibitor cocktail (Roche, Cat#11836170001)

FLAG antibody (Sigma Aldrich, Cat# SAB4200071)

Glyoxal solution (Merck, Cat#128465)

HindIII-HF (NEB, Cat# R3104S)

Hydrogen Peroxide (Acros Organics, Cat#7722-84-1)

Klenow exo- (NEB, Cat#M0212L)

Microscopy chamber with 8 individual wells high glass bottom (Thistle Scientific, Cat# IB-80807)

MOPS running buffer 20x (Invitrogen, NP0001)

Nitrocellulose membrane (Thermo Scientific, Cat#88018)

NotI-HF (NEB, Cat# R3189S)

NuPAGE Bis-Tris 4-12% precast gradient gels (Invitrogen, Cat#NP0321BOX)

OneShot Top10 Chemically competent E. coli (Thermo Scientific, Cat#C404003)

Phusion High-Fidelity DNA polymerase (NEB, Cat# M0530S)

Random hexamers (Thermo Scientific, Cat# 10609275)

RNasin (Promega, Cat# N2511)

RQ1 DNase (Promega, Cat# M6101)

Superscript III RT, 0.1M DTT, 5x First Strand Buffer (Invitrogen, Cat#18080093)

SwaI (NEB, Cat#R0604S)
T4 DNA ligase (NEB, Cat# M0202L)
TRIzol Reagent (Invitrogen, Cat#15596026)
Venus primary antibody (Agrisera, Cat# AS184227)
Yeast Nitrogen Base (Formedium, Cat#CYN0410)
Zirconia beads (Thiste Scientific, Cat#ZrOB05)

Commercial kits

Gel extraction kit (QIAGEN, Cat#28704)
Min Elute PCR purification kit (QIAGEN, Cat#28004)
Plasmid miniprep (ZYMO Research, Cat# D4016)
RNA clean & concentrator kit (ZYMO Research, Cat# R1013)
Zymoclean Gel DNA recovery kit (ZYMO Research, Cat# D4007)

Oligonucleotides

All oligonucleotides used in this study are listed in Supplementary Table 1.

Strains

All strains generated in this study are listed in Supplementary Table 2 and are available from the lead contact upon request.

Plasmids

All plasmids generated in this study are listed in Supplementary Table 3 and are available from the lead contact upon request.

Deposited data

reCRAC and RNAseq raw data

Software and Algorithms

BEdtools [59]
EdgeR [60]
Flexbar [61]
ggplot2 [62]
IGV [63]
Metamorph software (Molecular Devices)
Novoalign (V2.07.00, Novocraft Technologies)
GraphPad Prism Version 10.0.3

Proteomaps[36]
pyCRAC [64]
PyMOL 3.1(Molecular Graphics System)
Salmon[65]

METHOD DETAILS

Yeast cell culture and media

All Saccharomyces cerevisiae strains used in this paper originated from the BY4741 background (MATa his3Δ1 leu2Δ0 met15Δ0 ura3Δ0). Yeast cultures were grown in a growth medium containing 2% D-glucose, 2% yeast nitrogen base, and a 2% complement of amino acids excluding tryptophan (SD-Trp) at 30°C shaking. For all the experiments, the cultures were grown to a stationary phase overnight and then diluted the next morning from OD_{600} of 0.05 to OD_{600} of 0.45. For experimental treatments, yeast cells were either harvested directly from glucose-supplemented media (Glucose) or subjected to glucose deprivation by transferring to the same media but lacking glucose and instead supplemented with 2% glycerol and 2% ethanol (Glucose starvation). Only for the polysome profiling experiment, the cells were grown in a synthetic complete (SC) medium.

For reCRAC, cells were crosslinked with UVC at 254 nm at an OD_{600} of 0.45. Harvesting for both reCRAC, RNAseq and qPCR experiments involved rapid filtration of the cultures onto a nitrocellulose membrane, immediate immersion of the membrane into 50 mL of ice-cold water, centrifugation at 4,600 rpm for 2 min at 4°C, and subsequent freezing of the cell pellet.

Gene tagging, mutations and deletion

For reCRAC experiment, the chromosomal locus of Pin4 was modified to include an N-terminal FLAG-His (FH) tag. This tag consists of a FLAG sequence (GATTATAAAGATGAC GATGACAAG), a four-alanine spacer (GCCGCAGCCGCA), and a chain of eight histidines (CATCACCACCATCATCACCATCAC).

The integration of the FH tag was done using a CRISPR-Cas9 system, utilizing the pML104 plasmid as described [33]. This plasmid is engineered to include the Cas9 sequence, an ampicillin resistance gene, and the URA3 selection marker. It is also optimized for efficient and directional cloning of single guide (sg) RNA. The design features an sgRNA with a GATC overhang compatible for cloning, which is a 20-nucleotide guide sequence that targets genomic DNA (e.g. the N-terminus of Pin4), and a structural segment critical for Cas9 binding (see Supp. Table 1). The yeast CRISPR-Cas9 system stimulates homologous

recombination using a repair template that is co-transformed with the Cas9 and sgRNA expressing vector. This template includes homology regions close to the cleavage site, the sequence to be introduced/changed, and mutations either in the sgRNA target or in the adjacent PAM sequence (NGG) to confer resistance to further Cas9 cleavage in modified cells (see Supp. Table 1).

Briefly, for sgRNA preparation,10 µg of pML104 plasmid was digested overnight at room temperature with 2 µL of SwaI, subsequently inactivated at 65°C for 20 min, and further digested with 2 µL of BclI at 50°C for 2 hours. Following gel extraction with QIAGEN Gel extraction kit, the cut plasmid was ethanol precipitated, resuspended in water, aliquoted and stored at -80°C. The sgRNA oligos (Supp. Table 1) were annealed by combining 1 µM of each oligo with 1x T4 DNA ligase buffer in a total volume of 100 µL, heated at 95°C for 5 min, and then allowed to cool gradually to 20°C with the speed of 45s/°C. The annealed oligos were ligated with 66 ng of linearized pML104 plasmid using 0.5 µL T4 DNA ligase and 1x T4 DNA ligase buffer in a reaction volume of 10 µL. The mixture was kept at room temperature for 2 hours, transformed into OneShot Top10 Chemically Competent E. coli cells, and plated on LB-Amp plates. Plasmid DNA was isolated and sequenced to confirm the accurate sgRNA insertion in pML104 plasmid.

The FH tag was integrated using two repair templates consisting of the FH sequence flanked by 45 bp homology arms with engineered silent mutation to disrupt the PAM site, and 20 bp overlap at their 3' ends (Supp. Table 1). The repair template was made by annealing two 10 µM repair template oligos in 1x NEBuffer 2.1 in a reaction volume of 50 µL at 95°C for 6 min, and then decreasing the temperature by 1°C every 30s until 20°C was reached. The repair template was then extended with 1 µL of Klenow exo- together with 1.25 µL of 10 mM dNTPs for 1 hour at 37°C. 10 µL of the annealed and extended repair template was then co-transformed with 500 ng of sgRNA containing-pML104 plasmid into BY4741 strain using the standard PEG/LiOAc yeast protocol. Selection occurred twice on -URA plates, with further restreaking on YPD to remove the selection plasmids. Colonies were then restreaked on both YPD and -URA, and the ones that lost the pML104 plasmid and failed to grow on -URA were verified by PCR using the check oligos (Supp. Table 1) and sequenced for the correct insertion of the FH tag.

The pin4$_{RRM\Delta}$ strain, which involves deletion of the entire RRM domain from A86 to V158, and the pin4$_{RRM\text{-}M1}$ strain (V88A, L128A, F130A) was generated in the N-FH Pin4 background using the CRIRPS/Cas9 system, following the protocol described above. See Supp. Table 1 for the used oligos. For the complete deletion of the Pin4 gene, we employed

conventional homologous recombination, utilizing the KanMX6 cassette from the pFa6a plasmid (Addgene #39296), with oligonucleotides detailed in Supp. Table 1.

The Hsp104 protein was C-terminally tagged with GFP (S65T version) using a PCR-based method from the pFa6A plasmid (Addgene #39293), incorporating the KanMX6 selection marker (see Supp. Table 1). The resulting construct was transformed into the BY4741 strain and pin4$_{RRM\Delta}$ strain. The pin4$_{\Delta CT}$, where GFP was inserted after the first 200 amino acids of Pin4 was made by taking the GFP (S65T) from the pFa6A plasmid (Addgene #39293) and using it as the repair template utilizing CRISPR-Cas9 system as described above.

Growth curves

For the growth curves, yeast strains were inoculated from single colonies and grown overnight in SD-Trp medium. The cultures were then diluted to an optical density OD_{600} of 0.05 and grown to an OD_{600} of 0.45 in SD-Trp. At this exponential growth phase, cultures were diluted to an OD_{600} of 0.025 and 120 µL aliquots were pipetted into a 96-well plate. Stress-inducing agents were added to the wells at varying final concentrations: glyoxal at 0.3, 1,5, 3, 9 and 30 mM; and hydrogen peroxide at 0.5 and 1 mM. The 96-well plate was sealed with a sealing tape to minimize evaporation and placed in a Sunrise TECAN plate reader with a continuous shaking at 30°C. Optical density measurements were taken every 15 min to monitor growth. Each condition was tested in technical triplicate and biological duplicate. Specific strains are provided in the corresponding Fig. legends.

For the glucose starvation experiment, overnight saturated BY4741 and *pin4Δ* cells were diluted to an OD_{600} of 0.05 and grown to an OD_{600} of 0.40 in SD-Trp. Cells were then centrifuged, washed, resuspended in a medium containing 2% glycerol and 2% ethanol, and grown in this medium from an OD_{600} of 0.075. Growth was monitored over a period of 2.5 days. This condition was tested in a biological duplicate.

reCRAC

See Ristová et al,. (2024) for a detailed protocol and Fig. 1B for a visual overview of reCRAC. Briefly, Pin4 was engineered to include an N-terminal FLAG-4xAlanines-8xHistidines (FH) tag expressed from its native promoter to ensure it is the only variant produced. Expression of the tagged construct was verified by western blot (Supp. Fig. 3A). The strain was grown in SD-Trp, and upon reaching the exponential growth, cultures were UV crosslinked at 254 nm to stabilize RNA-protein interactions either in glucose medium or shifted to glucose-deprived medium (2%glycerol, 2% ethanol) for 16 min. The lysis step

involved highly denaturing conditions with 6 M Guanidine – HCl to prevent protein degradation, with subsequent purification step performed on Ni-NTA beads under similarly stringent conditions. The adapter ligation, radiolabeling with ^{32}P and partial Benzonase digestion to generate protein-protected RNA fragments were performed on the beads. Following elution from the Ni-NTA beads, a second purification on anti-FLAG beads was performed under more native conditions. The samples were then visualized via autoradiography, the RNA bound to the target protein was cut out and treated with Proteinase K. The RNA was then converted to cDNA, amplified and analyzed by high-throughput sequencing.

Reporter constructs

To study the effect of Pin4 binding on its RNA targets, we made reporter constructs using the modular cloning system (MoClo) [66]. This system involves assembling approximately nine modular parts (Part plasmids) – including different promoters, coding regions, terminators, etc. – in a manner similar to LEGO, creating a complete Cassette reporter plasmid in a single golden gate assembly reaction, which can be chromosomally integrated.

All toolkit Part plasmids except the terminator Part plasmids used in this study were obtained from Addgene and are found in Supp. Table 3. The terminator Part plasmids containing the sequences of 3' UTRs of Pin4 reCRAC targets (TPI1, GPM1) and a non-target control (PNC1) were generated for this study using PCR and standard cloning techniques.

The process to generate the terminator Part plasmids began by modifying the target terminator sequence to incorporate BsmBI and BsaI restriction sites via PCR amplification. This was done by extracting DNA from the parental By4741 strain using 100 µL of 200 mM LiOAc and 1% SDS solution. The sample was incubated at 70°C for 5 min, then precipitated with ethanol. The purified DNA then served as the template for PCR reactions using Phusion DNA Polymerase, with oligonucleotides listed in Supp. Table 1 (oligos #526, 527, 528, 529, 532, 533). We verified the PCR products on a 1% agarose gel, excised the appropriate bands, and purified the fragments using the Zymoclean Gel DNA Recovery Kit.

200 ng of the purified PCR products were digested with 0.5 µL of BsmBI-v2 in a total reaction volume of 40 µL for 2h at 55°C. The restriction enzyme was then heat deactivated at 80°C for 20 min. The reaction products were subsequently purified using the Min Elute PCR Purification Kit. We then ligated 80 ng of the digested inserts with 65 ng of the similarly treated empty entry vector (pYTK001) using 0.5 µL of T4 DNA ligase for 1.5h at room temperature. The ligase was inactivated by putting the samples at 65°C for 10 min. The

terminator Part plasmids were then transformed into NEB 5-alpha E. coli competent cells and plated onto LB- 25 µg/ml Chloroamphenicol plates, purified and verified by sequencing.

For assembling the complete Cassette plasmid, we combined individual Part plasmids in a reaction containing 74 ng of each part plasmid, 1 µL T4 DNA ligase, 2 µL T4 DNA ligase buffer, 1 µL BsaI in 20 µL volume reaction (see Supp. Table 3 for the detail of specific Part plasmids). The samples were incubated in a thermocycler with the setting of 25 cycles of 42°C for 2 min, 16°C for 5 min, with a final digestion step (60°C for 10 min) and heat inactivation (80°C for 10 min). The PCR products were then transformed into NEB 5 alpha E. coli competent cells. The assembly was verified by diagnostic digest using EcoRI-HF, NotI-HF, BamHI-HF, HindIII-HF restriction enzymes. Finally, the confirmed Cassette plasmids were linearized with NotI for 10 min at 37°C, transformed into target yeast strains (By4741, *pin4Δ*), which we plated on YPD plates with 600 µg/ml hygromycin. The integration into the chromosome was confirmed by PCR and sequencing using oligos listed in Supp. Table 1.

Western blot analysis of reporter constructs

For the analysis of the Venus reporter expression via western blot, cells expressing Venus reporters were initially grown overnight in SD-Trp medium. The following morning, the cultures were diluted to an OD_{600} of 0.05 and grown until reaching an OD_{600} of 0.45. Cells corresponding to 9 ODs were harvested by centrifugation at 4,600 rpm for 2 min and subsequently frozen at -90°C for storage. For glucose starvation experiments, cells were rapidly filtered and resuspended in a medium containing 2% glycerol and 2% ethanol, where they were incubated for 2 hours before spinning them and freezing them the same way as the non-starved samples.

Cell pellets were resuspended in 1 mL of 0.2 M NaOH and incubated on ice for 10 min. Subsequently, 100 µL of 50% trichloroacetic acid (TCA) was added to precipitate proteins. After mixing, samples were incubated on ice for an additional 10 min and then centrifuged at 14,000 rpm at 4°C for 10 min to pellet the precipitated proteins. The pellet was resuspended in 35 µL of lysis buffer (0.1 M Tris-HCl pH 6.8, 4 mM EDTA pH 8.0, 4% SDS, 20% glycerol, 2% β-mercaptoethanol). To adjust the pH, 15 µL of 1M Tris base was added to each sample. Samples were then heated at 95°C for 10 min and centrifuged at 10,000 rpm at room temperature for 10 min. The supernatant was kept, and the protein concentration was quantified using the Bradford assay. 25 µg of protein per sample was loaded onto a 4-12% Bis-Tris gel and subjected to electrophoresis at 180V for 1 hour in MOPS buffer. Proteins were then transferred to a nitrocellulose membrane using the i-blot2 system set on the P0 setting. Post-transfer, the membrane was stained with Ponceau S solution for 5 min to

visualize total protein transfer and subsequently blocked with 5% milk in PBS for 30 min. The membrane was incubated with primary antibodies against Venus (Agrisera AS18 4227, diluted in 1:1000) and Act1 (Abcam 8224, diluted 1:10,000) for 1 hour. After washing three times for 5 min each with PBS-T (0.1% tween), the membrane was incubated with a fluorescently labelled secondary antibody (LiCor, diluted 1:5,000 in 5% milk PBS-T) for 1 hour. Following three additional washes with PBS-T (0.1% tween), the membrane was scanned using the LI-COR software (LI-COR Biosciences). Act1 served as the loading control, the quantification was done using the ImageStudio (LI-COR Biosciences).

RNAseq

BY4741 and *pin4Δ* cells were cultured in 100 mL of SD-Trp to OD_{600} of 0.45 from OD_{600} of 0.05. Cells were rapidly filtered and immediately immersed in 50 mL of ice-cold water, centrifuged at 4,600 rpm for 2 min at 4°C, and the cell pellet was snap-frozen in a dry-ice and ethanol bath, and stored at -80°C. For glucose starvation stress, cells were incubated in SD-Trp medium without glucose but supplemented with 2% glycerol and 2% ethanol. At the 16 min timepoint, cells were filtered and immersed in 50 mL of ice-cold water, after which they were spun down as described for glucose samples, and snap-frozen. Biological triplicates were collected for each condition.

RNA was extracted from 10 OD_{600} units of cells using TRIzol reagent with the addition of 0.5% final β-mercaptoethanol. Cells were lysed by bead beating in screw-cap tubes three times in a Fast Prep-24 machine (MP Biomedicals) using 200 µL of Zirconia beads at a setting of 6 m/s for 40 sec. RNA was cleaned twice by chloroform extraction and precipitation was performed using 0.8 vol isopropanol. RNA concentration was quantified using Nanodrop (OD_{280}). 6 µg of RNA was treated with DNase I for 30 min and further purified using RNA Clean and Concentrator kit.

Libraries for RNAseq were prepared by the Edinburgh Clinical Research Facility at the Institute of Genetics and Cancer (Edinburgh, UK). RNA integrity and quality were assessed using an Agilent 2100 Electrophoresis Bioanalyser Instrument (Agilent Technologies Inc, #G2939AA) with RNA 6000 Nano chips (#5067-1511). RNA quantification was performed with Qubit 2.0 Fluorometer (Thermo Fisher Scientific Inc, #Q32866) using the Qubit RNA broad range assay kit (#Q10210). DNA contamination levels were evaluated using the Qubit dsDNA HS assay kit (#Q32854).

Libraries were prepared from 500 ng of total RNA per sample using the NEBNEXT Ultra II Directional RNA Library Prep kit (NEB #7760) and the Poly-A mRNA Magnetic Isolation

Module (NEB #E7490) following the manufacturer's protocols. Sequencing was carried out on the NextSeq 2000 platform (Illumina Inc, #20038897) using NextSeq 2000 P3 Reagents (200 Cycles) (#20040560) with paired-end, 2x 100 nt outputs.

Quantitative PCR (qPCR)

Yeast strains BY4741, *pin4Δ*, pin4$_{RRMΔ}$, pin4$_{RRM-M1}$, and Pin4$_{ΔCT}$ were cultured overnight in SD-Trp medium. The next day, cultures were diluted to an OD_{600} of 0.05 and grown in 100 mL of SD-Trp to an OD_{600} of 0.45. For glucose starvation experiments, cells were filtered and resuspended in 100 mL of medium containing 2% glycerol and 2% ethanol for 16 or 32 min. For harvesting, cultures were rapidly filtered, and the cells were immediately immersed in 50 mL of ice-cold water, centrifuged at 4,600 rpm for 2 min at 4°C, and cell pellets were frozen.

For RNA extraction, cell pellets corresponding to 10 OD_{600} units were lysed using 100 µL of TRIzol reagent in the presence of 200 µL zirconia beads and 0.5% β-mercaptoethanol. The lysis was performed in screw-cap tubes twice using a fast prep machine at 6 m/s for 40 seconds. Extra 500 µL of TRIzol reagent with 0.5% β-mercaptoethanol were added and the bead beating was repeated one more time. The samples were cleared by centrifugation, and RNA was extracted using a chloroform-isopropanol method. The RNA was washed with 70-75% ethanol, dried and resuspended in DNase/RNase-free water. The RNA concentration was quantified using a Nanodrop spectrophotometer.

For reverse transcription, the extracted RNA was first treated to remove any contaminating genomic DNA. 15 µg of RNA was mixed with 7 µL of RQ1 DNase and 1x buffer, along with 1 µL of RNasin. This mixture was gently vortexed and incubated at 37°C for 30 min. The DNase was then inactivated by adding 125 µL of water to the mixture, followed by an extraction with equal volume of phenol:chloroform:isoamyl alcohol (25:24:1), vortexed vigorously, and centrifuged at 12,000g for 10 min at 4°C. The aqueous phase was extracted, treated with chloroform and isoamyl alcohol (24:1), and the RNA was precipitated overnight at -20°C using sodium acetate and ethanol. The RNA pellet was washed, dried, and dissolved in DNase/RNase-free water. The concentration and purity of RNA were assessed using a Nanodrop spectrophotometer.

Reverse transcription was performed on 1 µg of DNase-treated RNA using random hexamers and Superscript III Reverse Transcriptase (Invitrogen). The reaction mixture included 0.2 µg/µL random hexamers, 10 mM dNTP mix, 5x first-strand buffer, 0.1M DTT, RNasin, and reverse transcriptase. The mixture was incubated at 65°C for 5 min, followed by synthesis conditions of 25°C for 15 min, 55°C for 1 hour, and a final inactivation step at 70°C

for 15 min. Finally, 180 µL of water was added to the reaction to obtain a total volume of 200 µL of cDNA.

Quantitative PCR was carried out in triplicate using SYBR Green I master mix (Roche) on an MX3005P qPCR system (Agilent Technologies). Each 10 µL reaction contained 4 µL of cDNA, 5 µL of 2x SYBR Green master mix, 0.4 µL of 10 µM primers (forward and reverse mixed at 1:1), 0.04 µL of Rox II and 0.56 µL water. The thermal cycling conditions were as follows: initial denaturation at 95°C for 30 seconds, followed by 38 cycles of 95°C for 5 seconds, 55°C for 15 seconds, and 72°C for 15 seconds.

Microscopy

Saccharomyces cerevisiae strains expressing Hsp104-C-GFP in the WT background, and Hsp104-C-GFP in pin4$_{RRM\Delta}$ background were cultured in 20 mL of SD-Trp medium from OD_{600} of 0.05 to OD_{600} of 0.45. After reaching this optical density, 175 µL of cell suspension was put onto a chambered coverslip with eight individual wells (Thistle Scientific) that has been pre-coated with 10 µL of Concanavalin A (ConA, 5 mg/mL stock) for 10 min at 32°C and subsequently washed three times with SD-Trp medium. Cells were allowed to adhere to the coverslip surface for 20 min at 32°C. Following adhesion, non-adherent cells were removed with three washes using 500 µL of SD-Trp medium. The adherent cells were then imaged at 25 °C using a spinning disc confocal microscope with a Nikon TE2000 microscope base, a modified Yokogawa CSU-10 spinning disk (Visitech) an iXon + Du888 EMCCD camera (Andor) and a 100x/1.45 NA Plan Apo objective (Nikon). For glucose starvation monitoring, the cells were washed three times with 500 µL of glucose-starvation medium (SD-Trp without glucose, supplemented with 2% glycerol and 2% ethanol), and imaged for further 2-hour period. Metamorph software (Molecular Devices) were used to capture images every three min with an exposure time of 150 ms, 488 nm laser set at 35% power and a 0.6 µm step-size over 11 z-sections at three-minute intervals.

Polysome profiling

WT and *pin4Δ* cells were grown in SD-Trp medium overnight to obtain the saturated cultures the following morning. Thes cultures were then diluted in 100 mL of SD-Trp and grown in synthetic complete (SC) medium from OD_{600} of 0.05 to OD_{600} of 0.45. Cycloheximide was added to the cultures at a final concentration of 0.1 mg/mL for 5 min before harvesting to stabilize ribosomes by blocking them during elongation phase. Cells were subsequently pelleted by centrifugation at 4,600 rpm for 2 min at 4°C, washed once with 20 mL of ice-cold water, snap-frozen in a dry-ice and ethanol bath, and stored at -80°C. Biological duplicates

were collected for each condition. For glucose starvation experiments, when reaching the right OD, cells were initially filtered and transferred to 100 mM of SC medium supplemented with 2% glycerol and 2% ethanol instead of glucose, for 16 min. The cells were then harvested as described above.

Following the methodology outlined in Winz et al. (2019)[67], cell lysis was performed by resuspending cell pellets in 300 µL of lysis buffer (20 mM HEPES-KOH pH 7.4, 100 mM potassium acetate, 2 mM magnesium acetate and EDTA-free protease inhibitors). The suspension was transferred to screw-cap tubes containing 200 µL of zirconia beads prepared on ice and subjected to four cycles of bead beating using a Fast Prep-24 machine (MP Biomedicals) set at 6m/s for 40 seconds with a pre-cooled cool adapter. For each of the beating, 8g of dry ice was used to keep the samples cold, but not freezing. An additional 200 µL of lysis buffer was added post-bead beating, and the lysate was cleared twice for 15 min at maximum speed at 4°C. RNA concentration was measured on a Nanodrop spectrophotometer.

300 µg of RNA was loaded onto 10%-45% sucrose gradients made in 1x gradient buffer (10 mM Tris-acetate pH 7.4, 70 mM ammonium acetate, 2 mM magnesium acetate). Gradients were first made using a Gradient Master (BioComp) set to the “Short; SW40; Suc10-45%” program and refrigerated for 2 hours. After loading the RNA on the gradients, the gradients were centrifuged at 38,000 rpm for 2.5 hours at 4°C in SW40-Ti rotors using an Optima XPN-100 Ultracentrifuge (Beckmann Coulter) with acceleration set at 1 and deceleration at 9. Post-centrifugation, gradients were fractionated into 60 fractions of 200 µL each using a Piston Gradient Fractionator (BioComp), equipped with a TRIAX flow cell (BioComp) for UV profiling and an FC203B fraction collector (Gilson).

QUANTIFICATION AND STATISTICAL ANALYSIS

Protein domain analysis of Pin4

Regions within Pin4 matching protein domain families were identified using the NCBI Conserved Domains database, which revealed predicted RNA recognition motif (RRM) and R3H domains. Domain alignments and phylogenetics trees were constructed based on the information available on the same platform. 3D structure prediction for Pin4 was performed using AlphaFold3.

AlphaFold3 modelling was carried out with two copies of the full-length sequences of Pin4 from *S. cerevisiae* [27]. After inspection, a sequence encompassing the R3H was also modelled, also with two copies (residues 273-373; R3H designated as residues 306-367).

The predicted aligned error was visualised using PAE viewer [68] and figures were generated using Pymol.

reCRAC sequence data analysis

Sequencing of reCRAC libraries was done on the Illumina MiniSeq system, using the High Output Reagent Cartridge. Bioinformatic analysis of reCRAC followed the protocol described by Ristová et al., 2024. Initially, reads were demultiplexed using pyBarcodeFilter.py based on uniquely barcoded 5' linkers. Quality filtering and 3' adapter trimming were done using Flexbar with specified settings (--removal-tags -at RIGHT -ao 4 -u 3 -m 7 -n 16 -t), and targeting the adapter sequence TGGAATTCTCGGGTGCCAAGGC. PCR duplicates were removed using pyFastqDuplicateRemover.py, which collapses reads with identical three random nucleotide sequences present in the 5' linker. These collapsed FASTA reads were then aligned to the Saccharomyces cerevisiae reference genome (SGD v64) using Novoalign (V2.07.00, Novocraft) with Ensembl annotations (EF4.74), applying the Random -r method. Read quantification was executed with pyReadCounters.py, using the Ensembl GTF version EF4.74, which includes mRNA annotations with UTRs, as well as different non-coding RNA categories such as CUTs and SUTs.

The output of pyReadCounters.py is a read count file (hittable). One pseudocount was added to each transcript to improve quantification. The reads were RPM normalized due to a very specific Pin4 binding peak and the normalized data were plotted against RPKM normalized RNAseq data. For the distribution of binding, the ratio between 5'UTR, CDS, 3' UTR over the genomic region was calculated, mean value from the three replicates was taken with SD.

Most analysis were done on transcripts that showed the strongest Pin4 binding, for these an arbitrary cut off of at least 0.3% of the library was made from the raw reads. Protein binding sites were visualized using the Integrative Genomics Viewere (IGV). For this purpose, reads aligned with Novoalign were converted from SAM to BAM format, which were then sorted and indexed using samtools. Read normalization was achieved by calculating a scaling factor relative to the library size, and coverage was determined using bedtools for each strand, producing scaled bedgraph files for loading onto IGV. The pyPileup.py tool was utilized to illustrate the distribution of reads with number of deletions and substitutions, which represent the sites of protein-RNA crosslinks, along the TPI1, GPM1 and ALT2 genes. The motif sequence was found by taking the targets that make up 0.3% of the library, identified the highest deletion peak and taking 10 nt from upstream and downstream from this peak and searched for enriched motifs using MEME. 2D plotter was used to generate a metagene

plot of reads aligned to their 3' end. Scatter plots and bar graphs were created using GraphPad Prism 9. Gene ontology representations were generated via the Proteomaps website. Bar graphs display the median values from three experimental replicates, with error bars representing the standard deviation (SD).

RNA-seq analysis

The paired-end Illumina RNA-seq data were first pre-processed using Flexbar to trim low quality bases and adapters from raw reads. The specific parameters set for Flexbar included quality filtering of tail bases with a quality threshold of 30 (Sanger scale), adapter removal with a minimum overlap of four bases, and discarding of reads shorter than 18 bases after trimming (-q TAIL -qf sanger -qt 30 -aa TruSeq -ao 4 -m 18 -n 16). The cleaned reads were then aligned to the *S. cerevisiae* transcriptome using Salmon [65] to quantify transcript abundances. For this, the genome GTF file and FASTA files for genes, cDNAs, and ncRNAs were downloaded from Ensembl (version GCF_000146045.2_R64-1-1). These files were used with Salmon's generateDecoyTranscriptome.sh script to create a hybrid FASTA containing decoy genome sequences concatenated with the transcriptome. Indices for this decoy-aware transcriptome were built using the Salmon indexer. The salmon quant command was then employed to quantify the processed reads against this index. The resulting data were imported into R and processed with the edgeR package. Reads were normalized using the Trimmed Mean of M-values (TMM) method [69]. Data filtering was performed using the 'filterByExp' function in edgeR, applying a count per million (CPM) threshold with a minimum count per sample of 15 and a minimum total count of 30.

The experimental design was modelled using the 'model.matrix' function in R, which accounted for both sample variations and replicates. Dispersion estimates were obtained using 'estimateDisp', and generalized linear models (GLM) were fit to the data using the 'glmQLFit' function employing a quasi-likelihood approach. Differential expression analysis was subsequently performed using 'glmQLFTest'. Visualisation of differentially expressed genes, heatmaps, volcano plots, was performed using ggplot2, with significant genes being identified based on a fold change threshold of 2 and a false discovery rate (FDR) of 0.05. PCA plots were made using the log transformed CPM normalized data.

For comparative analysis with reCRAC data, RNAseq datasets of the WT under normal and glucose starvation conditions were mapped using Novoalign to generate SAM files. These files were then processed to produce bedgraph files as described in the **reCRAC sequence data analysis** section. Visualization of these data was facilitated using the Integrative Genomics Viewer.

qPCRs

Each sample was measured in a technical and biological triplicate and a median was taken for the results. The relative expression levels were calculated using the ΔΔCt method with a housekeeping gene (ALG9) as the reference. Data were normalized to the control condition and expressed as fold changes. Bar graphs show the average of three replicates and error bars show SD or SEM. Detailed information is provided in the Fig. captions. GraphPad Prism 9 software was used for the statistical analyses.

Microscopy Image Processing and Analysis

Raw microscopy pictures were processed using ImageJ software (Fiji; NIH). Displayed images represent maximum projections of 11 z-sections with a 0.6 µm step-size. To quantitatively assess the presence of Hsp104 protein granules, cells were categorized as either containing or lacking visible granules at each time point. The percentage of cells with at least one granule was calculated and graphically represented using GraphPad Prism 9 software together with the statistical test .

Figure 1B was made using BioRender.

ACKNOWLEDGEMENTS

We thank Richard Clark from Clinical Research Facility Edinburgh for sequencing services; Shaun Webb and Ola Helwak for answering all our extensive bioinformatics questions; and Adam Kováč and Ye Dee Tay for their help with the spinning disc confocal microscope and with the analysis and processing of raw data images. We thank Ola Helwak and Sophie Giguere for the critical reading of this manuscript. MR was supported by an EASTBIO PhD fellowship [543KOM/G40389]. KB was supported by Wellcome Trust PhD Studentship [218470]. VS and DT were supported by Wellcome Principal Research Fellowships [109916, 222516]. AGC was supported by a Wellcome Senior Fellowship [200898]. This work was facilitated by funding for the Wellcome Discovery Research Platform for Hidden Cell Biology [226791] and we gratefully acknowledge support from the Microscopy and Bioinformatics cores. Work in the Wellcome Centre for Cell Biology was supported by Centre Core Grants (092076 and 203149).

FIGURE LEGENDS

Figure 1: Identification of the Pin4 RNA-bound interactome

A) Pin4 is a largely unstructured protein with three predicted domains, an RNA Recognition Motif (RRM), a coiled-coil domain (CC), and an R3H domain. The previously identified prion-forming domain is also annotated. The RRM and R3H domain regions belong to two protein domain families: RRM_PIN4_like and R3H_RRM respectively. B) Overview of the reCRAC technique. Briefly, yeast cells were irradiated at 254 nm to induce covalent crosslinks (yellow stars) between proteins and associated RNAs. Cells were lysed in denaturing conditions, to prevent protein degradation and reduce non-specific interactions. The bait protein carries a FLAG-His_8 tag, allowing purification on Ni-NTA beads, where the enzymatic steps of RNA digestion and radiolabeling and linker ligation (red star) were performed. This was followed by elution and purification on Anti-FLAG beads. Complexes were gel-purified, the radioactive RNA visualized by autoradiography and the region corresponding to the RNA-protein complexes excised. The bait protein was treated with Proteinase K, leaving one or more residual aminoacids. RNA was extracted, converted to cDNA by reverse transcription (RT), and sequenced. See the methods section for more detail [35]. Figure created with BioRender. C) Total reads recovered in reCRAC libraries from Glucose and No glucose conditions (16 min in Gly/EtOH) for FH-Pin4 and Untagged control. Each condition was analyzed in triplicate. The Untagged background control had minimal number of reads as expected. D) The relative fraction of reCRAC reads belonging to Glucose and No glucose (16 min in Gly/EtOH) Pin4 libraries. The experiment was performed in triplicate for each condition.

Figure 2: Pin4 predominantly targets a single motif in 3' UTRs

A) Distribution of Pin4 binding to 5'UTR, CDS, and 3' UTR of target mRNAs in Glucose and No glucose (16 min in Gly/EtOH) conditions. RNAseq was included as a control. Pin4 targets mainly 3' UTRs in both conditions. B) Metagene plot showing the total hits across Pin4 reCRAC data aligned to the 3' end in Glucose (blue) and No glucose (orange) conditions. The highest peak is present close to the 3' end in both conditions, but substantially lower following glucose depletion. C) Examples of FH-Pin4 binding across its top targets (*TPI1*, *ILV5*, *GPM1*, *RPS12*). Three replicates are plotted on top of each other, each shown in a different color shade. RNA-seq is shown for comparison. The reads are normalized to the size of the library and scaled to the highest peak in Pin4 reCRAC and RNAseq. The autoscaled Pin4 reCRAC peaks are shown on right next to the plots. D) Pin4 motif (MEME) in DNA alphabet found in the 3' UTR of Pin4 targets (mRNA species that individually comprise ≥ 0.3% of the total library) in Glucose (35 RNAs) and No glucose (38 RNAs) conditions. The E value is given below each motif. E) Close up view of reCRAC pileups of

the 3' UTR of Pin4 target, *ADH1*, in Glucose and No glucose conditions. The motif sequence TA/TATGA/T is marked in red and underlined. The deletion peaks (orange) represent the sites of crosslinks between RNA and protein.

Figure 3: Pin4 binding is enriched on metabolic and growth-associated mRNAs
A-B) Scatterplots comparing the changes in Pin4-RNA binding versus the mRNA abundance in Glucose and No glucose (16 min in Gly/EtOH) conditions. The zoomed in window shows the top Pin4-RNA enriched targets colored based on their GO term enrichment. C) Scatterplot showing the top mRNA Pin4 targets (≥ 0.3% of the total library) in glucose and glucose depletion (16 min) conditions. The transcripts fall into four GO term enrichment categories: glycolysis, mitochondrial and amino acid metabolism, and translation. D) Bar graphs showing the percentage of the total Pin4 reCRAC library, in glucose or glucose delpeted, together with the RNAseq control. Mean and individual replicates are plotted. Error bars show SEM (n=3). E-F) Box plots showing scaled, relative abundances of top Pin4-RNA targets (≥ 0.3% of the total library) identified under different GO terms relative to RNAseq. Significant differences between conditions were calculated with the Mann-Whitney statistical test and are indicated by asterisks (* $p < 0.05$, ** $p < 0.01$, **** $p < 0.0001$). Individual replicate values are plotted.

Figure 4: Pin4 negatively regulates the abundance of target mRNAs
A) Volcano plot of differential gene expression analysis in *pin4Δ* compared to the WT under glucose conditions. Significantly downregulated and upregulated genes are highlighted in red (adj. p value ≤ 0.05, log2FC ≥ 2). B) Heatmap showing the expression of top Pin4-RNA targets in WT and *pin4Δ* under glucose condition. Each row represents a different gene and each column represents a different experimental replicate. Expression levels are color-coded from blue (low expression) to red (high expression) and normalized. C) Schematic representation of the reporter construct used in this study. The construct contains the P_{TEF2} promoter, driving the expression of the Venus fluorescent protein, which is fused to the 3' UTR from top Pin4-RNA targets: *TPI1* and *GPM1*. *PNC1* terminator sequence was used as a control. D) Bar graphs showing the levels of RNA (left) and protein (right) for specific genes (*TPI1* and *GPM1*) that are targets of Pin4 regulation, alongside a control (*PNC1*). Data are represented for WT and *pin4Δ* strains under glucose and glucose depletion conditions (16 min for RNA levels (n=3), 2 hr for protein levels (n=2)). Values are normalized to the WT in glucose (dark blue). Significance was calculated using Mann Whitney two-tailed test. Individual replicate values are plotted. E) Bar graphs depicting the mRNA levels of *TPI1* and *GPM1* in WT and *pin4Δ* in glucose and glucose depletion conditions as determined from

RNAseq and normalized by counts per million (CPM) (n=3, mean values and replicates plotted; error bars represent SD). Each dot represents an individual replicate. Statistical analyses were performed using EdgeR and significant differences were observed with FDR-adjusted p-values of 2.60×10^{-8} and 1.98×10^{-11} for TPI1 in glucose and glucose depletion between WT and *pin4Δ* strains, respectively, and 2.43×10^{-7} and 3.31×10^{-9} for GPM1. Mean and individual replicates are plotted. F) Scatterplot showing the relationship between RNA-seq log2FC of gene expression in *pin4Δ* compared to WT in glucose and Pin4-RNA binding in this condition. Each point represents a gene. R^2 value of 0.0056 is shown for the line of best fit.

Figure 5: Loss of Pin4 blocks transcriptional responses to glucose depletion

A) Principal component analysis (PCA) depicting the variation in gene expression profiles between the WT and *pin4Δ* with and without glucose (16 min in Gly/EtOH). Each point represents a biological replicate, showing the distinct clustering of each group based on their overall gene expression. B) Spearman correlation heatmap showing pairwise comparisons of gene expression between WT and *pin4Δ* under different conditions. The heatmap colors represent Spearman correlation coefficients, indicating the degree of similarity between the conditions. C) Heatmap of gene expression across WT and *pin4Δ* strain in glucose and glucose depletion conditions. Genes are clustered by the rows, based on expression patterns. The color scale represents expression levels from low (blue) to high (red). D) Volcano plot of differential gene expression analysis in *pin4Δ* compared to the WT under glucose depletion conditions (16 min in Gly/EtOH). Significantly downregulated and upregulated genes are highlighted in red (adj. p value ≤ 0.05, log2FC ≥ 2). E) Bubble chart representing the GO term enriched biological processes among mRNAs with increased levels in *pin4Δ* relative to the WT. The size of each bubble indicates the gene count, while the color reflects the p-value. Gene ratio is defined as the proportion of differentially expressed genes (DEGs) that are present in a particular gene set, divided by the total number of DEGs. F) As E but showing mRNAs with reduced levels in *pin4Δ*.

Figure 6: Pin4 RRM and prion-forming domains are critical for the transcriptional response to glucose depletion

A) Schematics of representation of constructs, $pin4_{RRM\Delta}$, lacking the RRM domain, $pin4_{RRM\text{-}M1}$ with mutated RRM domain (in red), and $pin4_{\Delta CT}$ (green). B) Bar graphs comparing RNA expression levels determined by qRT-PCR normalized to *ALG9*, for strains carrying WT *PIN4*, *pin4Δ,* $pin4_{RRM\Delta}$ or $pin4_{RRM\text{-}M1}$ in glucose medium and following glucose depletion for 16 or 32 min (n=3, mean with SEM). Individual replicate values are plotted. C) As B but with

strains WT *PIN4*, *pin4Δ,* pin4$_{RRMΔ}$ or pin4$_{ΔCT}$, with glucose depleted for 16 min. Values are plotted as a fold change to WT in glucose conditions (*** $p < 0.001$, **** $p < 0.0001$; n=3, mean with SEM). Ordinary one-way ANOVA with Dunnett's multiple comparisons test was used for the statistical test. Individual replicate values are plotted.

Figure 7: Loss of the Pin4 RRM reduces Hsp104 granule formation

A) Microscopy images showing the expression of Hsp104-GFP for WT and pin4$_{RRMΔ}$ strains in glucose and following glucose depletion for 30, 60, or 120 min. B-C) Bargraphs showing the percentage of cells with visible Hsp104-GFP foci in WT and pin4$_{RRMΔ}$ strains over a time course following glucose depletion. Blue bars represent the temporal dynamics of Hsp104 granule formation in WT cells, and orange bars in pin4$_{RRMΔ}$ cells. Statistical significance is indicated (*** $p < 0.001$, **** $p < 0.0001$, ns = not significant). Ordinary one-way ANOVA with Dunnett's multiple comparisons test was used for the statistical test. Mean and individual replicate values are plotted.

Figure 8: Model for Pin4 function

During growth in glucose, Pin4 functions in post-transcriptional gene regulation by specific binding to the 3' UTR of mRNA targets, predominantly linked to metabolic and pro-growth processes, favoring their destabilization. Following glucose withdrawal, mRNA binding by Pin4 is greatly decreased. Binding remains 3' UTR enriched for some transcripts but includes coding sequences of mRNAs related to translation. Pin4 is also required to activate the transcriptional response to glucose deprivation. The mechanism is not yet determined, but both the prion-forming domain and RNA recognition motif (RRM) of Pin4 are necessary. This indicates that the transcriptional stress response is subject to riboregulation.

Supplementary Figure 1: Domain structure of Pin4

A) Multiple sequence alignment of the conserved domains of Pin4: RRM_PIN4_like and R3H_RRM domains across various species. The conserved residues are colored, and the beginning and end of both the RRM and R3H domains are annotated. RNP1 and RNP2 motifs within RRM are also annotated. B) Phylogenetic trees depicting the evolutionary relationship of the RRM_PIN4_like and R3H_RRM domain containing proteins. The fungi are highlighted in orange, and the protozoan species in blue.

Supplementary Figure 2: Pin4 RRM domain is non-canonical and R3H may homodimerize

A) Comparison of RRM motifs between the canonical RRM and Pin4 RRM. The diagram indicates critical amino acid positions and sequences within RNP1 and RNP2 of the canonical RRM, and alterations in Pin4. B) Modelled 3D structure of the Pin4 RRM domain, Non-consensus amino acids, L128, F130 (RNP1), and V88 (RNP2) are highlighted in red. C) AlphaFold3 prediction of the R3H domain dimer from Pin4. The domains are colored in red or pink and the residues at the N and C terminal positions of this fragment are marked with residue numbers. PAE matrix for models with the R3H domains alone modelled as a dimer. D) AlphaFold3 prediction of dimeric Pin4, with RRM domains colored light and bright orange, coiled coil (CC) regions colored light and bright cyan, and R3H domains colored red and pink. Note that the R3H domain modeled here extends beyond the annotation in Figure 1A (residues 273-373). The N and C termini are marked with blue and dark red spheres, respectively. Probability scores (ipTM and pTM) are marked. Predicted aligned error matrix (PAE) for full-length Pin4 modelled as a dimer. The area of the matrix corresponding to the predicted R3H interaction is marked with a salmon-colored box.

Supplementary Figure 3: Analysis of Pin4-RNA interactions with reCRAC

A) Western blot (left) and autoradiograph (right) analysis showing the protein expression and protein-RNA crosslinking of N-terminal FLAG-Ala_4-His_8 tagged (N-FH) Pin4 during CRAC and reCRAC experiments. L, lysate; NE, Ni-NTA eluate; FE, FLAG eluate. The untagged control expresses endogenous Pin4 without the tag. The red boxes indicate the regions excised for further steps. B) Heatmap of Pearson correlation coefficients for N-FH-Pin4 and untagged reCRAC samples performed across glucose and glucose depletion conditions performed in triplicate. The heatmap colors range from blue (low correlation) to red (high correlation). C) Principal component analysis (PCA) of RPM normalized reCRAC data for all RNA classes across different strains and conditions. D) Bar chart displaying the relative fraction of reCRAC reads recovered in No glucose (16 min in Gly/EtOH) from N-FH-Pin4 and untagged strains. The experiment was performed in triplicate for each condition. E) Bar chart of N-FH-Pin4 reCRAC targets following glucose depletion. The data are grouped based on 3'UTR and CDS association (y-axis) and the number of mRNA targets is plotted on the x-axis. Gene ontology enrichment is given for each group. F) The zoomed-in view of reCRAC pileups of the 3' UTR of Pin4 targets, *TDH3*, *ILV5*, and *PDC1* in glucose rich and glucose-poor conditions. The motif sequence TA/TATGA/T is marked in red. The deletion peaks (orange) represent the sites of crosslinking between RNA and protein

Supplementary Figure 4: Pin4 targets are enriched for metabolic and pro-growth mRNAs

A) GO term enrichment across all Pin4 targets in glucose condition (n=3), and RNAseq data in glucose condition (n=3). Each bubble represents a transcript, and the size of the bubble determines the enrichment of that transcript in a library. Figure prepared using the Proteomaps tool [36]. B) Scatterplots showing the top Pin4 target mRNAs in glucose and glucose depletion (16 min Gly/EtOH) conditions that represented at least 0.3% of the Pin4 reCRAC library comparing all the replicates. The mRNAs are enriched for four GO term categories: glycolysis, mitochondrial, amino acid metabolism, and translation.

Supplementary Figure 5: Pin4 deficient cells are sensitive to glucose depletion and mitochondrial stress

A) Growth curves of the WT and *pin4Δ* strains in the presence of glucose (n=2, mean value plotted). Absorbance was measured over 45 hr to measure growth. B) Growth curves of WT and *pin4Δ* strains during following transfer from glucose medium to medium with Gly/EtOH (n=2, mean value plotted). Absorbance was measured over 70 hr. C) Bar chart showing the doubling time and lag phase in hours following shift from glucose to Gly/EtOH. D) Growth curves of WT and *pin4Δ* strain exposed to medium containing varying concentrations of hydrogen peroxide (H_2O_2) (n=2, mean value plotted). E) Comparison of doubling time and lag phase of WT and *pin4Δ* strain exposed to 0.5 mM and 1 mM H_2O_2. F) Growth curves showing the WT and *pin4Δ* in 9 mM glyoxal (n=2, mean value plotted). G) Doubling times of WT and *pin4Δ* strains in medium supplemented different concentrations of glyoxal (n=2).

Supplementary Figure 6: Altered mRNAs and reporters in *pin4Δ*

A-B) Bubble charts of GO term enrichment of biological process or molecular function, among mRNAs with increased or decreased abundance in *pin4Δ* relative to the WT in glucose medium. The size of each bubble indicates the gene count, while the color reflects the p-value. Gene ratio is defined as the proportion of differentially expressed genes (DEGs) that are present in a particular gene set, divided by the total number of DEGs. C) Western blots of the Venus reporters with terminator sequences obtained from *GPM1*, *TPI1*, or *PNC1* gene in glucose or glucose depletion (2 hr Gly/EtOH) conditions. The Venus level was normalized to an Actin loading control.

Supplementary Figure 7: Altered mRNAs in *pin4Δ* and RRM mutant growth curves

A-B) Bubble charts of GO term enrichment of cellular component or molecular function among mRNAs with increased or decreased abundance in *pin4Δ* relative to the WT following glucose depletion (16 min Gly/EtOH). The size of each bubble indicates the gene count, while the color reflects the p-value. Gene ratio is defined as the proportion of differentially

expressed genes (DEGs) that are present in a particular gene set, divided by the total number of DEGs. C) *G*rowth curve of WT, *pin4Δ*, pin4$_{RRM\Delta}$, and pin4$_{RRM\text{-}M1}$ in glucose medium. D) Polysome profile analysis of WT and *pin4Δ* in glucose (blue) and no glucose (16 min in Gly/EtOH) conditions (orange).

REFERENCES

1. Fulda, S., Gorman, A.M., Hori, O., and Samali, A. (2010). Cellular Stress Responses: Cell Survival and Cell Death. Int. J. Cell Biol. *2010*, 214074. https://doi.org/10.1155/2010/214074.

2. Gebauer, F., Schwarzl, T., Valcárcel, J., and Hentze, M.W. (2020). RNA-binding proteins in human genetic disease. Nat. Rev. Genet., 1–14. https://doi.org/10.1038/s41576-020-00302-y.

3. Goswami, B., Nag, S., and Ray, P.S. (2024). Fates and functions of RNA-binding proteins under stress. WIREs RNA *15*, e1825. https://doi.org/10.1002/wrna.1825.

4. Galdieri, L., Mehrotra, S., Yu, S., and Vancura, A. (2010). Transcriptional Regulation in Yeast during Diauxic Shift and Stationary Phase. OMICS J. Integr. Biol. *14*, 629–638. https://doi.org/10.1089/omi.2010.0069.

5. Liberti, M.V., and Locasale, J.W. (2016). The Warburg Effect: How Does it Benefit Cancer Cells? Trends Biochem. Sci. *41*, 211–218. https://doi.org/10.1016/j.tibs.2015.12.001.

6. Alfarouk, K.O., Verduzco, D., Rauch, C., Muddathir, A.K., Adil, H.H.B., Elhassan, G.O., Ibrahim, M.E., David Polo Orozco, J., Cardone, R.A., Reshkin, S.J., et al. (2014). Glycolysis, tumor metabolism, cancer growth and dissemination. A new pH-based etiopathogenic perspective and therapeutic approach to an old cancer question. Oncoscience *1*, 777–802.

7. Cazzulo, J.J. (1992). Aerobic fermentation of glucose by trypanosomatids. FASEB J. *6*, 3153–3161. https://doi.org/10.1096/fasebj.6.13.1397837.

8. Tadege, M., and Kuhlemeier*, C. (1997). Aerobic fermentation during tobacco pollen development. Plant Mol. Biol. *35*, 343–354. https://doi.org/10.1023/A:1005837112653.

9. Pfeiffer, T., and Morley, A. (2014). An evolutionary perspective on the Crabtree effect. Front. Mol. Biosci. *1*. https://doi.org/10.3389/fmolb.2014.00017.

10. Hernández-Elvira, M., and Sunnerhagen, P. (2022). Post-transcriptional regulation during stress. FEMS Yeast Res. *22*, foac025. https://doi.org/10.1093/femsyr/foac025.

11. Chang, Y., and Huh, W.-K. (2018). Ksp1-dependent phosphorylation of eIF4G modulates post-transcriptional regulation of specific mRNAs under glucose deprivation conditions. Nucleic Acids Res. *46*, 3047–3060. https://doi.org/10.1093/nar/gky097.

12. Heinrich, S., Hondele, M., Marchand, D., Derrer, C.P., Zedan, M., Oswald, A., Malinovska, L., Uliana, F., Khawaja, S., Mancini, R., et al. (2024). Glucose stress causes

mRNA retention in nuclear Nab2 condensates. Cell Rep. *43*, 113593. https://doi.org/10.1016/j.celrep.2023.113593.

13. Kuhn, K.M., DeRisi, J.L., Brown, P.O., and Sarnow, P. (2001). Global and Specific Translational Regulation in the Genomic Response of Saccharomyces cerevisiae to a Rapid Transfer from a Fermentable to a Nonfermentable Carbon Source. Mol. Cell. Biol. *21*, 916–927. https://doi.org/10.1128/MCB.21.3.916-927.2001.

14. Ashe, M.P., De Long, S.K., and Sachs, A.B. (2000). Glucose Depletion Rapidly Inhibits Translation Initiation in Yeast. Mol. Biol. Cell *11*, 833–848.

15. Kayikci, Ö., and Nielsen, J. (2015). Glucose repression in Saccharomyces cerevisiae. FEMS Yeast Res. *15*, fov068. https://doi.org/10.1093/femsyr/fov068.

16. Kim, J.-H., Roy, A., Jouandot, D., and Cho, K.H. (2013). The glucose signaling network in yeast. Biochim. Biophys. Acta *1830*, 5204–5210. https://doi.org/10.1016/j.bbagen.2013.07.025.

17. Rolland, F., Winderickx, J., and Thevelein, J.M. (2002). Glucose-sensing and -signalling mechanisms in yeast. FEMS Yeast Res. *2*, 183–201. https://doi.org/10.1111/j.1567-1364.2002.tb00084.x.

18. Conrad, M., Schothorst, J., Kankipati, H.N., Van Zeebroeck, G., Rubio-Texeira, M., and Thevelein, J.M. (2014). Nutrient sensing and signaling in the yeast Saccharomyces cerevisiae. FEMS Microbiol. Rev. *38*, 254–299. https://doi.org/10.1111/1574-6976.12065.

19. Bresson, S., Shchepachev, V., Spanos, C., Turowski, T.W., Rappsilber, J., and Tollervey, D. (2020). Stress-Induced Translation Inhibition through Rapid Displacement of Scanning Initiation Factors. Mol. Cell *80*, 470-484.e8. https://doi.org/10.1016/j.molcel.2020.09.021.

20. Bresson, S., Shchepachev, V., and Tollervey, D. (2023). A posttranscriptional pathway regulates cell wall mRNA expression in budding yeast. Cell Rep. *42*, 112184. https://doi.org/10.1016/j.celrep.2023.112184.

21. Pike, B.L., and Heierhorst, J. (2007). Mdt1 facilitates efficient repair of blocked DNA double-strand breaks and recombinational maintenance of telomeresv. Mol. Cell. Biol. *27*, 6532–6545. https://doi.org/10.1128/MCB.00471-07.

22. Pike, B.L., Yongkiettrakul, S., Tsai, M.D., and Heierhorst, J. (2004). Mdt1, a novel Rad53 FHA1 domain-interacting protein, modulates DNA damage tolerance and G(2)/M cell cycle progression in Saccharomyces cerevisiae. Mol. Cell. Biol.

23. Derkatch, I.L., Bradley, M.E., Hong, J.Y., and Liebman, S.W. (2001). Prions Affect the Appearance of Other Prions: The Story of [PIN+]. Cell *106*, 171–182. https://doi.org/10.1016/S0092-8674(01)00427-5.

24. Wang, J., Chitsaz, F., Derbyshire, M.K., Gonzales, N.R., Gwadz, M., Lu, S., Marchler, G.H., Song, J.S., Thanki, N., Yamashita, R.A., et al. (2022). The conserved domain database in 2023. Nucleic Acids Res. *51*, D384–D388. https://doi.org/10.1093/nar/gkac1096.

25. Yang, Z., Stone, D.E., and Liebman, S.W. (2014). Prion-promoted phosphorylation of heterologous amyloid is coupled with ubiquitin-proteasome system inhibition and toxicity. Mol. Microbiol. *93*, 1043–1056. https://doi.org/10.1111/mmi.12716.

26. Yang, Z., Hong, J.Y., Derkatch, I.L., and Liebman, S.W. (2013). Heterologous Gln/Asn-Rich Proteins Impede the Propagation of Yeast Prions by Altering Chaperone Availability. Plos Genet. *9*, e1003236. https://doi.org/10.1371/journal.pgen.1003236.

27. Abramson, J., Adler, J., Dunger, J., Evans, R., Green, T., Pritzel, A., Ronneberger, O., Willmore, L., Ballard, A.J., Bambrick, J., et al. (2024). Accurate structure prediction of biomolecular interactions with AlphaFold 3. Nature *630*, 493–500. https://doi.org/10.1038/s41586-024-07487-w.

28. Martín, V., Rodríguez-Gabriel, M.A., McDonald, W.H., Watt, S., Yates, J.R., Bähler, J., and Russell, P. (2006). Cip1 and Cip2 Are Novel RNA-Recognition-Motif Proteins That Counteract Csx1 Function during Oxidative Stress. Mol. Biol. Cell *17*, 1176–1183. https://doi.org/10.1091/mbc.E05-09-0847.

29. Maris, C., Dominguez, C., and Allain, F.H.-T. (2005). The RNA recognition motif, a plastic RNA-binding platform to regulate post-transcriptional gene expression. FEBS J. *272*, 2118–2131. https://doi.org/10.1111/j.1742-4658.2005.04653.x.

30. He, G.-J., Zhang, A., Liu, W.-F., and Yan, Y.-B. (2013). Distinct roles of the R3H and RRM domains in poly(A)-specific ribonuclease structural integrity and catalysis. Biochim. Biophys. Acta BBA - Proteins Proteomics *1834*, 1089–1098. https://doi.org/10.1016/j.bbapap.2013.01.038.

31. Liu, W.-F., Zhang, A., He, G.-J., and Yan, Y.-B. (2007). The R3H domain stabilizes poly(A)-specific ribonuclease by stabilizing the RRM domain. Biochem. Biophys. Res. Commun. *360*, 846–851. https://doi.org/10.1016/j.bbrc.2007.06.139.

32. Heierhorst, J. (2008). Mdt1/ASCIZ: A new DNA damage response protein family. Cell Cycle *7*, 2654–2660. https://doi.org/10.4161/cc.7.17.6593.

33. Laughery, M.F., Hunter, T., Brown, A., Hoopes, J., Ostbye, T., Shumaker, T., and Wyrick, J.J. (2015). New vectors for simple and streamlined CRISPR–Cas9 genome editing in Saccharomyces cerevisiae. Yeast *32*, 711–720. https://doi.org/10.1002/yea.3098.

34. Granneman, S., Kudla, G., Petfalski, E., and Tollervey, D. (2009). Identification of protein binding sites on U3 snoRNA and pre-rRNA by UV cross-linking and high-throughput analysis of cDNAs. Proc. Natl. Acad. Sci. U. S. A. *106*, 9613–9618. https://doi.org/10.1073/pnas.0901997106.

35. Ristova, M., Shchepachev, V., and Tollervey, D. (2024). reCRAC: A Stringent Method for Precise Mapping of Protein-RNA Interactions in Yeast. Preprint at bioRxiv, https://doi.org/10.1101/2024.05.22.594286.

36. Liebermeister, W., Noor, E., Flamholz, A., Davidi, D., Bernhardt, J., and Milo, R. (2014). Visual account of protein investment in cellular functions. Proc. Natl. Acad. Sci. U. S. A. *111*, 8488–8493. https://doi.org/10.1073/pnas.1314810111.

37. Bähler, J., Wu, J.-Q., Longtine, M.S., Shah, N.G., Mckenzie III, A., Steever, A.B., Wach, A., Philippsen, P., and Pringle, J.R. (1998). Heterologous modules for efficient and versatile PCR-based gene targeting in Schizosaccharomyces pombe. Yeast *14*, 943–951. https://doi.org/10.1002/(SICI)1097-0061(199807)14:10<943::AID-YEA292>3.0.CO;2-Y.

38. Messner, C.B., Demichev, V., Muenzner, J., Aulakh, S.K., Barthel, N., Röhl, A., Herrera-Domínguez, L., Egger, A.-S., Kamrad, S., Hou, J., et al. (2023). The proteomic

landscape of genome-wide genetic perturbations. Cell *186*, 2018-2034.e21. https://doi.org/10.1016/j.cell.2023.03.026.

39. Chowdhury, M.N., Chen, X., and Jin, H. (2023). An intrinsically Disordered RNA Binding Protein Modulates mRNA Translation and Storage. bioRxiv, 2023.05.22.541713. https://doi.org/10.1101/2023.05.22.541713.

40. Calabretta, S., and Richard, S. (2015). Emerging Roles of Disordered Sequences in RNA-Binding Proteins. Trends Biochem. Sci. *40*, 662–672. https://doi.org/10.1016/j.tibs.2015.08.012.

41. Ottoz, D.S.M., and Berchowitz, L.E. (2020). The role of disorder in RNA binding affinity and specificity. Open Biol. *10*, 200328. https://doi.org/10.1098/rsob.200328.

42. Shorter, J., and Southworth, D.R. (2019). Spiraling in Control: Structures and Mechanisms of the Hsp104 Disaggregase. Cold Spring Harb. Perspect. Biol. *11*, a034033. https://doi.org/10.1101/cshperspect.a034033.

43. Sathyanarayanan, U., Musa, M., Bou Dib, P., Raimundo, N., Milosevic, I., and Krisko, A. (2020). ATP hydrolysis by yeast Hsp104 determines protein aggregate dissolution and size in vivo. Nat. Commun. *11*, 5226. https://doi.org/10.1038/s41467-020-19104-1.

44. Smolka, M.B., Albuquerque, C.P., Chen, S., and Zhou, H. (2007). Proteome-wide identification of in vivo targets of DNA damage checkpoint kinases. Proc. Natl. Acad. Sci. *104*, 10364–10369. https://doi.org/10.1073/pnas.0701622104.

45. Soufi, B., Kelstrup, C.D., Stoehr, G., Fröhlich, F., Walther, T.C., and Olsen, J.V. (2009). Global analysis of the yeast osmotic stress response by quantitative proteomics. Mol. Biosyst. *5*, 1337–1346. https://doi.org/10.1039/B902256B.

46. Gnad, F., de Godoy, L.M.F., Cox, J., Neuhauser, N., Ren, S., Olsen, J.V., and Mann, M. (2009). High-accuracy identification and bioinformatic analysis of in vivo protein phosphorylation sites in yeast. PROTEOMICS *9*, 4642–4652. https://doi.org/10.1002/pmic.200900144.

47. Soulard, A., Cremonesi, A., Moes, S., Schütz, F., Jenö, P., and Hall, M.N. (2010). The Rapamycin-sensitive Phosphoproteome Reveals That TOR Controls Protein Kinase A Toward Some But Not All Substrates. Mol. Biol. Cell *21*, 3475–3486. https://doi.org/10.1091/mbc.E10-03-0182.

48. Bodenmiller, B., Wanka, S., Kraft, C., Urban, J., Campbell, D., Pedrioli, P.G., Gerrits, B., Picotti, P., Lam, H., Vitek, O., et al. (2010). Phosphoproteomic Analysis Reveals Interconnected System-Wide Responses to Perturbations of Kinases and Phosphatases in Yeast. Sci. Signal. *3*, rs4. https://doi.org/10.1126/scisignal.2001182.

49. Helbig, A.O., Rosati, S., Pijnappel, P.W., van Breukelen, B., Timmers, M.H., Mohammed, S., Slijper, M., and Heck, A.J. (2010). Perturbation of the yeast N-acetyltransferase NatB induces elevation of protein phosphorylation levels. BMC Genomics *11*, 685. https://doi.org/10.1186/1471-2164-11-685.

50. Glauninger, H., Bard, J.A.M., Hickernell, C.J.W., Airoldi, E.M., Li, W., Singer, R.H., Paul, S., Fei, J., Sosnick, T.R., Wallace, E.W.J., et al. (2024). Transcriptome-wide mRNA condensation precedes stress granule formation and excludes stress-induced transcripts. Preprint at bioRxiv, https://doi.org/10.1101/2024.04.15.589678.

51. Teixeira, D., Sheth, U., Valencia-Sanchez, M.A., Brengues, M., and Parker, R. (2005). Processing bodies require RNA for assembly and contain nontranslating mRNAs. RNA *11*, 371–382. https://doi.org/10.1261/rna.7258505.

52. Zedan, M., Schürch, A.P., Heinrich, S., García, P.G., Khawaja, S., and Weis, K. (2024). Newly synthesized mRNA selectively escapes translational repression following acute stress. Preprint at bioRxiv, https://doi.org/10.1101/2024.04.14.589419.

53. Christoph Messner (2023). The Proteomic Landscape of Genome-Wide Genetic Perturbations. (Mendeley). https://doi.org/10.17632/W8JTMNSZD9.1.

54. Miller, J.E., Zhang, L., Jiang, H., Li, Y., Pugh, B.F., and Reese, J.C. (2017). Genome-Wide Mapping of Decay Factor–mRNA Interactions in Yeast Identifies Nutrient-Responsive Transcripts as Targets of the Deadenylase Ccr4. G3 GenesGenomesGenetics *8*, 315–330. https://doi.org/10.1534/g3.117.300415.

55. Schlecht, U., Miranda, M., Suresh, S., Davis, R.W., and St.Onge, R.P. (2012). Multiplex assay for condition-dependent changes in protein–protein interactions. Proc. Natl. Acad. Sci. U. S. A. *109*, 9213–9218. https://doi.org/10.1073/pnas.1204952109.

56. Tarassov, K., Messier, V., Landry, C.R., Radinovic, S., Molina, M.M.S., Shames, I., Malitskaya, Y., Vogel, J., Bussey, H., and Michnick, S.W. (2008). An in Vivo Map of the Yeast Protein Interactome. Science *320*, 1465–1470. https://doi.org/10.1126/science.1153878.

57. Shangari, N., and O'Brien, P.J. (2004). The cytotoxic mechanism of glyoxal involves oxidative stress. Biochem. Pharmacol. *68*, 1433–1442. https://doi.org/10.1016/j.bcp.2004.06.013.

58. Uvdal, P., and Shashkova, S. (2023). The Effect of Calorie Restriction on Protein Quality Control in Yeast. Biomolecules *13*, 841. https://doi.org/10.3390/biom13050841.

59. Quinlan, A.R., and Hall, I.M. (2010). BEDTools: a flexible suite of utilities for comparing genomic features. Bioinformatics *26*, 841–842. https://doi.org/10.1093/bioinformatics/btq033.

60. Robinson, M.D., McCarthy, D.J., and Smyth, G.K. (2010). edgeR: a Bioconductor package for differential expression analysis of digital gene expression data. Bioinformatics *26*, 139–140. https://doi.org/10.1093/bioinformatics/btp616.

61. Dodt, M., Roehr, J.T., Ahmed, R., and Dieterich, C. (2012). FLEXBAR—Flexible Barcode and Adapter Processing for Next-Generation Sequencing Platforms. Biology *1*, 895. https://doi.org/10.3390/biology1030895.

62. Wickham, H. (2016). ggplot2 (Springer International Publishing) https://doi.org/10.1007/978-3-319-24277-4.

63. Robinson, J.T., Thorvaldsdóttir, H., Winckler, W., Guttman, M., Lander, E.S., Getz, G., and Mesirov, J.P. (2011). Integrative Genomics Viewer. Nat. Biotechnol. *29*, 24–26. https://doi.org/10.1038/nbt.1754.

64. Webb, S., Hector, R.D., Kudla, G., and Granneman, S. (2014). PAR-CLIP data indicate that Nrd1-Nab3-dependent transcription termination regulates expression of

hundreds of protein coding genes in yeast. Genome Biol. *15*, R8. https://doi.org/10.1186/gb-2014-15-1-r8.

65. Patro, R., Duggal, G., Love, M.I., Irizarry, R.A., and Kingsford, C. (2017). Salmon provides fast and bias-aware quantification of transcript expression. Nat. Methods *14*, 417–419. https://doi.org/10.1038/nmeth.4197.

66. Lee, M.E., DeLoache, W.C., Cervantes, B., and Dueber, J.E. (2015). A Highly Characterized Yeast Toolkit for Modular, Multipart Assembly. ACS Synth. Biol., 12.

67. Winz, M.-L., Peil, L., Turowski, T.W., Rappsilber, J., and Tollervey, D. (2019). Molecular interactions between Hel2 and RNA supporting ribosome-associated quality control. Nat. Commun. *10*, 563. https://doi.org/10.1038/s41467-019-08382-z.

68. Elfmann, C., and Stülke, J. (2023). PAE viewer: a webserver for the interactive visualization of the predicted aligned error for multimer structure predictions and crosslinks. Nucleic Acids Res. *51*, W404–W410. https://doi.org/10.1093/nar/gkad350.

69. Robinson, M.D., and Oshlack, A. (2010). A scaling normalization method for differential expression analysis of RNA-seq data. Genome Biol. *11*, R25. https://doi.org/10.1186/gb-2010-11-3-r25.

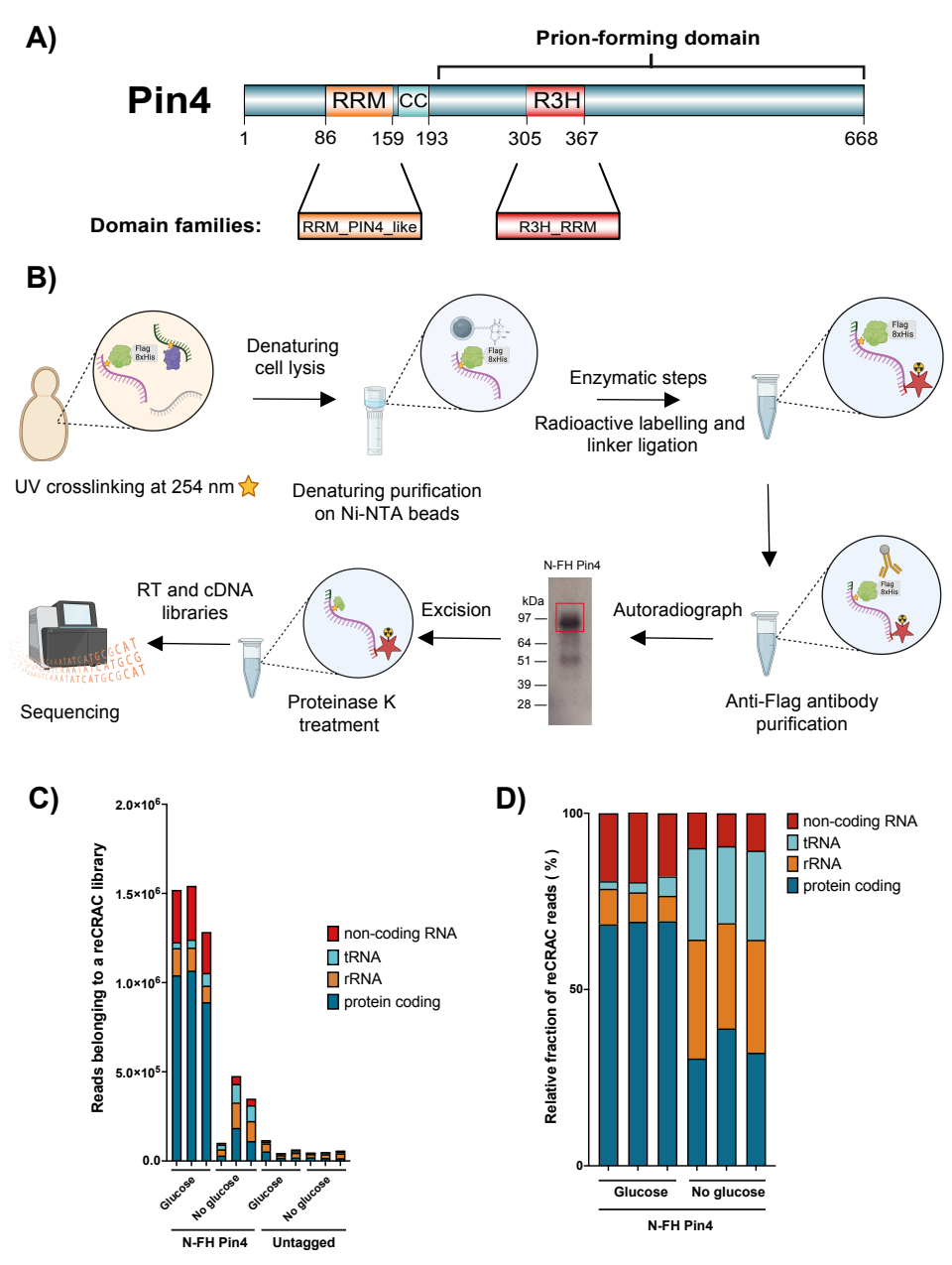
A)
Prion-forming domain
Pin4
RRM
CC
R3H
1
86
159
193
305
367
668
Domain families:
RRM_PIN4_like
R3H_RRM
B)
Flag
8xHis
Denaturing
cell lysis
Enzymatic steps
Radioactive labelling and
linker ligation
UV crosslinking at 254 nm
Denaturing purification
on Ni-NTA beads
N-FH Pin4
kDa
97
64
51
39
28
RT and cDNA
libraries
Excision
Autoradiograph
Sequencing
Proteinase K
treatment
Anti-Flag antibody
purification
C)
Reads belonging to a reCRAC library
2.0×10^6
1.5×10^6
1.0×10^6
5.0×10^5
0.0
non-coding RNA
tRNA
rRNA
protein coding
Glucose
No glucose
Glucose
No glucose
N-FH Pin4
Untagged
D)
Relative fraction of reCRAC reads (%)
100
50
0
non-coding RNA
tRNA
rRNA
protein coding
Glucose
No glucose
N-FH Pin4

Figure 1

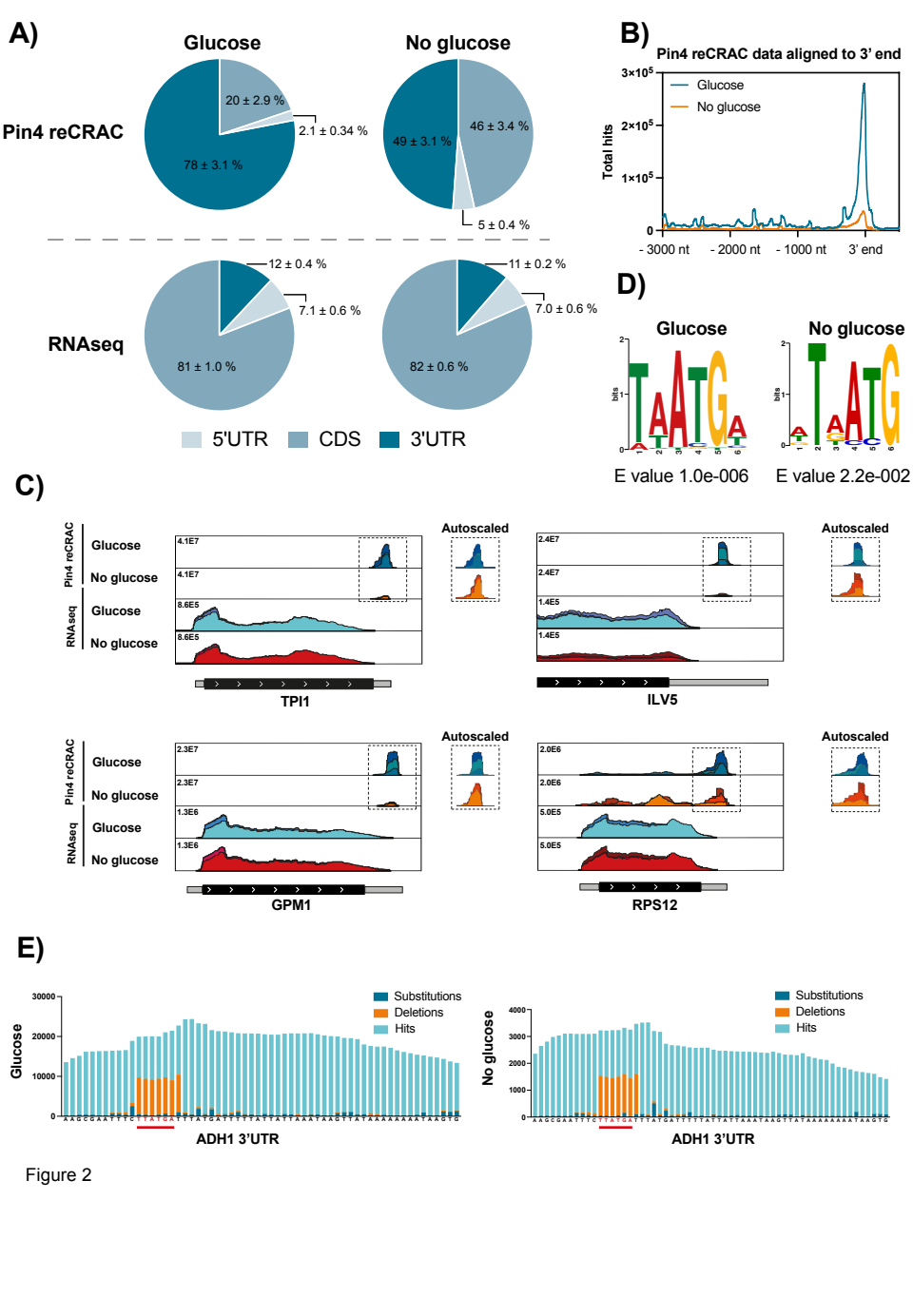
A)
Glucose
No glucose
Pin4 reCRAC
20 ± 2.9 %
2.1 ± 0.34 %
78 ± 3.1 %
46 ± 3.4 %
49 ± 3.1 %
5 ± 0.4 %
RNAseq
12 ± 0.4 %
7.1 ± 0.6 %
81 ± 1.0 %
11 ± 0.2 %
7.0 ± 0.6 %
82 ± 0.6 %
5'UTR
CDS
3'UTR
B)
Pin4 reCRAC data aligned to 3' end
Glucose
No glucose
Total hits
3×10^5
2×10^5
1×10^5
0
- 3000 nt
- 2000 nt
- 1000 nt
3' end
D)
Glucose
No glucose
bits
E value 1.0e-006
E value 2.2e-002
C)
Pin4 reCRAC
RNAseq
Glucose
No glucose
Autoscaled
TPI1
ILV5
GPM1
RPS12
E)
Glucose
No glucose
Substitutions
Deletions
Hits
ADH1 3'UTR

Figure 2

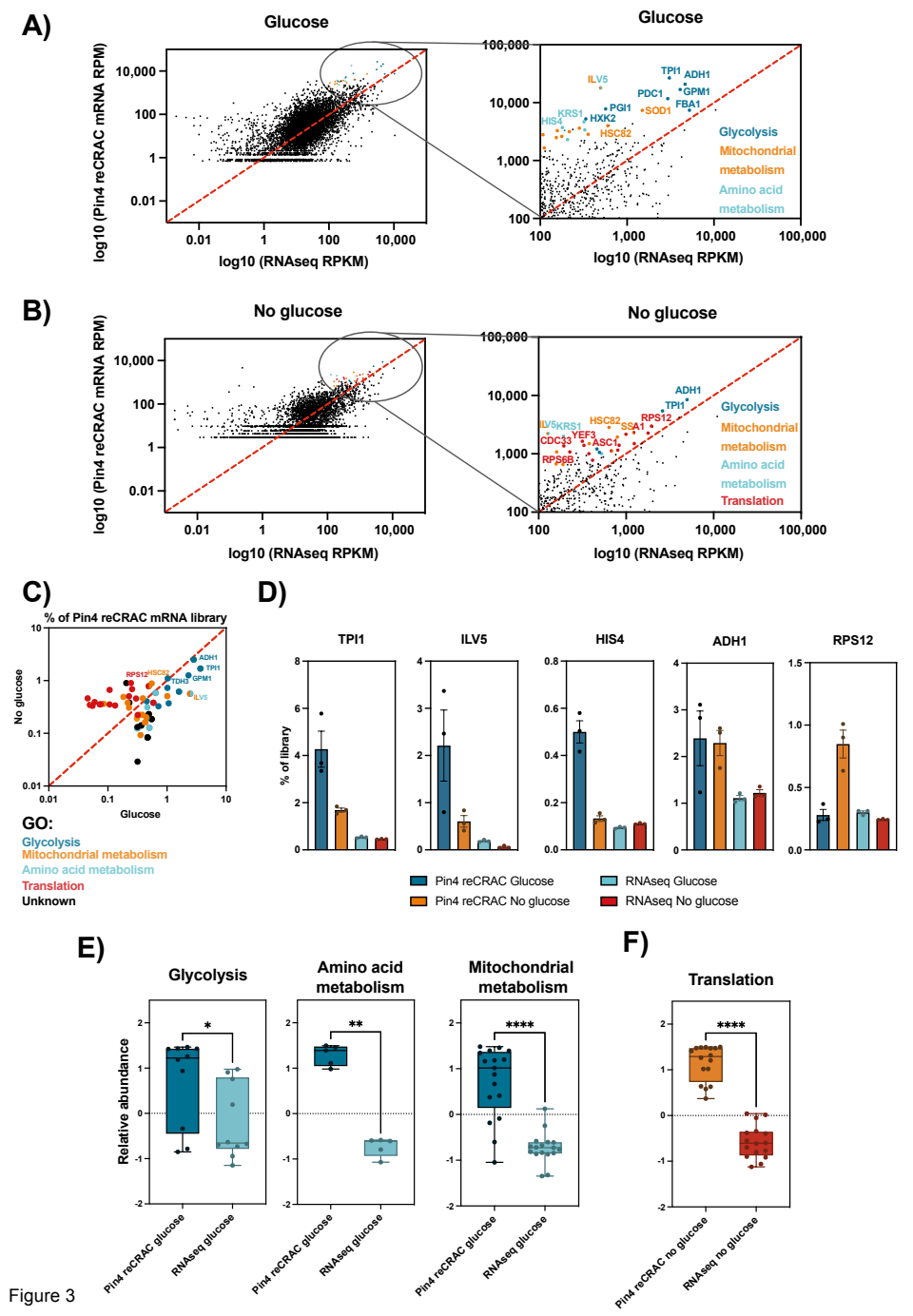
A)
Glucose
log10 (Pin4 reCRAC mRNA RPM)
log10 (RNAseq RPKM)
ILV5
TPI1
ADH1
PDC1
GPM1
FBA1
SOD1
PGI1
HXK2
KRS1
HIS4
HSC82
Glycolysis
Mitochondrial metabolism
Amino acid metabolism
B)
No glucose
ADH1
TPI1
RPS12
ILV5
KRS1
HSC82
SSA1
YEF3
CDC33
ASC1
RPS6B
Translation
C)
% of Pin4 reCRAC mRNA library
No glucose
Glucose
RPS12
HSC82
ADH1
TPI1
TDH3
GPM1
ILV5
GO:
Glycolysis
Mitochondrial metabolism
Amino acid metabolism
Translation
Unknown
D)
TPI1
ILV5
HIS4
ADH1
RPS12
% of library
Pin4 reCRAC Glucose
Pin4 reCRAC No glucose
RNAseq Glucose
RNAseq No glucose
E)
Glycolysis
Amino acid metabolism
Mitochondrial metabolism
Relative abundance
Pin4 reCRAC glucose
RNAseq glucose
F)
Translation
Pin4 reCRAC no glucose
RNAseq no glucose

Figure 3

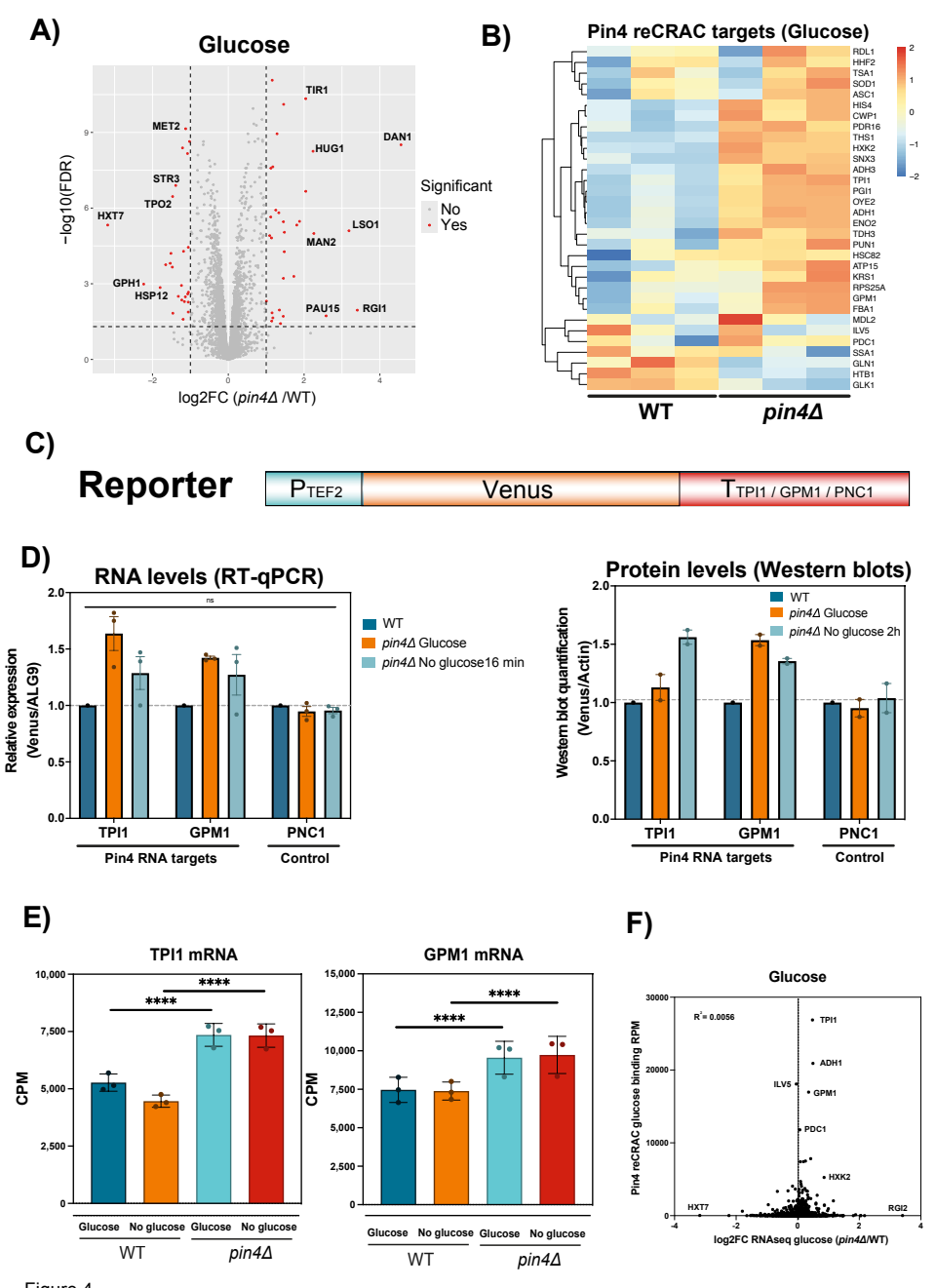
A)
Glucose
TIR1
MET2
DAN1
HUG1
STR3
TPO2
HXT7
LSO1
MAN2
GPH1
HSP12
PAU15
RGI1
Significant
No
Yes
−log10(FDR)
log2FC (pin4Δ /WT)
B)
Pin4 reCRAC targets (Glucose)
RDL1
HHF2
TSA1
SOD1
ASC1
HIS4
CWP1
PDR16
THS1
HXK2
SNX3
ADH3
TPI1
PGI1
OYE2
ADH1
ENO2
TDH3
PUN1
HSC82
ATP15
KRS1
RPS25A
GPM1
FBA1
MDL2
ILV5
PDC1
SSA1
GLN1
HTB1
GLK1
WT
pin4Δ
C)
Reporter
PTEF2
Venus
TTPI1 / GPM1 / PNC1
D)
RNA levels (RT-qPCR)
ns
WT
pin4Δ Glucose
pin4Δ No glucose16 min
Relative expression (Venus/ALG9)
TPI1
GPM1
PNC1
Pin4 RNA targets
Control
Protein levels (Western blots)
WT
pin4Δ Glucose
pin4Δ No glucose 2h
Western blot quantification (Venus/Actin)
TPI1
GPM1
PNC1
Pin4 RNA targets
Control
E)
TPI1 mRNA
****
****
CPM
Glucose
No glucose
Glucose
No glucose
WT
pin4Δ
GPM1 mRNA
****
****
CPM
Glucose
No glucose
Glucose
No glucose
WT
pin4Δ
F)
Glucose
R² = 0.0056
TPI1
ADH1
ILV5
GPM1
PDC1
HXK2
HXT7
RGI2
Pin4 reCRAC glucose binding RPM
log2FC RNAseq glucose (pin4Δ/WT)

Figure 4

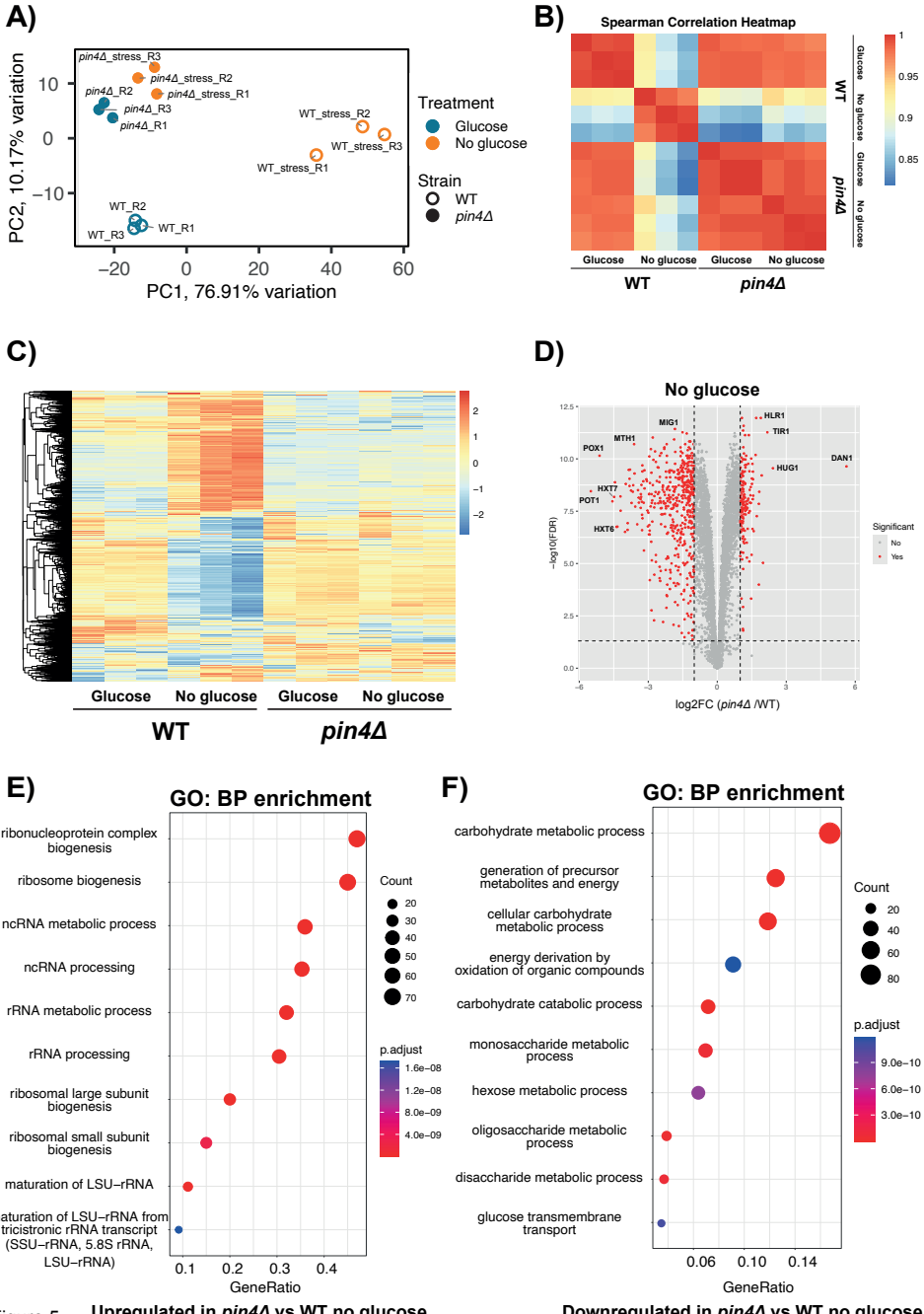
A)
PC2, 10.17% variation
PC1, 76.91% variation
pin4Δ_stress_R3
pin4Δ_stress_R2
pin4Δ_stress_R1
pin4Δ_R2
pin4Δ_R3
pin4Δ_R1
WT_stress_R2
WT_stress_R3
WT_stress_R1
WT_R2
WT_R3
WT_R1
Treatment
Glucose
No glucose
Strain
WT
pin4Δ
B)
Spearman Correlation Heatmap
Glucose
No glucose
WT
pin4Δ
C)
Glucose
No glucose
WT
pin4Δ
D)
No glucose
HLR1
TIR1
MIG1
MTH1
POX1
DAN1
HUG1
HXT7
POT1
HXT6
−log10(FDR)
log2FC (pin4Δ /WT)
Significant
No
Yes
E)
GO: BP enrichment
ribonucleoprotein complex biogenesis
ribosome biogenesis
ncRNA metabolic process
ncRNA processing
rRNA metabolic process
rRNA processing
ribosomal large subunit biogenesis
ribosomal small subunit biogenesis
maturation of LSU−rRNA
maturation of LSU−rRNA from tricistronic rRNA transcript (SSU−rRNA, 5.8S rRNA, LSU−rRNA)
GeneRatio
Count
p.adjust
Upregulated in pin4Δ vs WT no glucose
F)
GO: BP enrichment
carbohydrate metabolic process
generation of precursor metabolites and energy
cellular carbohydrate metabolic process
energy derivation by oxidation of organic compounds
carbohydrate catabolic process
monosaccharide metabolic process
hexose metabolic process
oligosaccharide metabolic process
disaccharide metabolic process
glucose transmembrane transport
GeneRatio
Count
p.adjust
Downregulated in pin4Δ vs WT no glucose

Figure 5

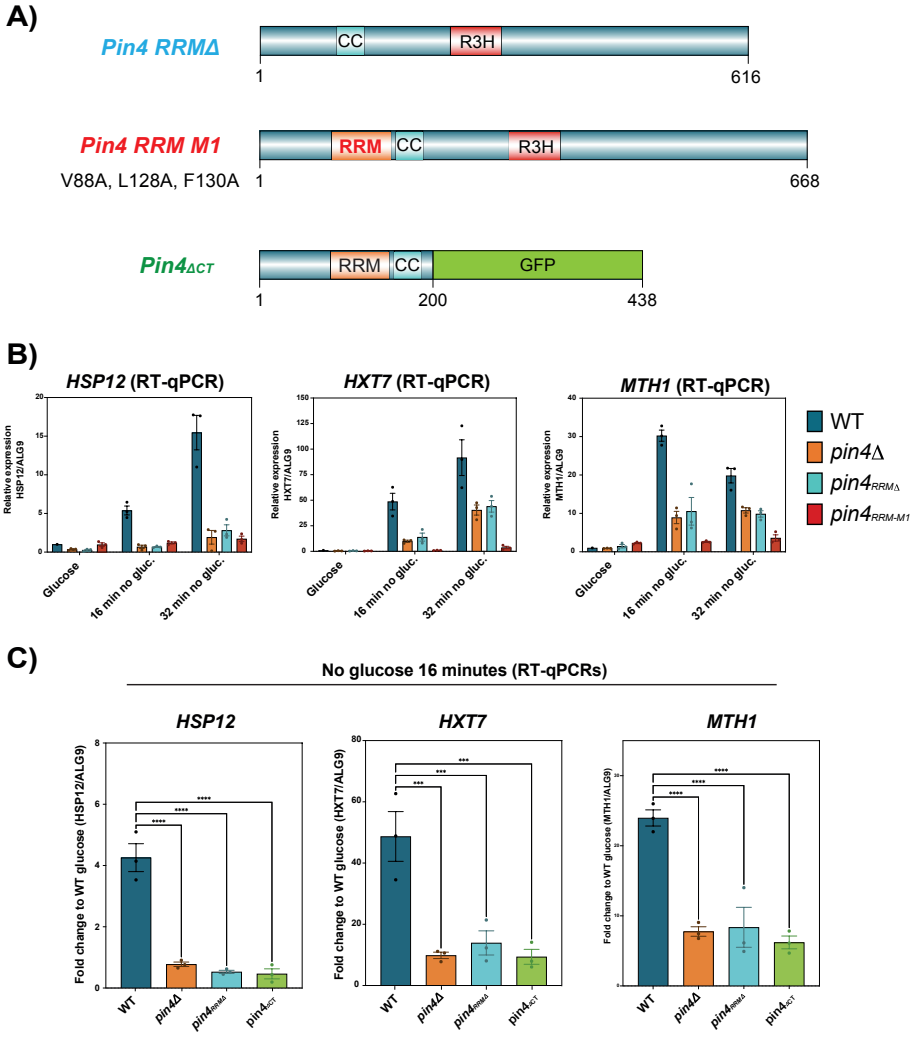
A)
Pin4 RRMΔ
CC
R3H
1
616
Pin4 RRM M1
V88A, L128A, F130A
RRM
CC
R3H
1
668
Pin4ΔCT
RRM
CC
GFP
1
200
438
B)
HSP12 (RT-qPCR)
HXT7 (RT-qPCR)
MTH1 (RT-qPCR)
Relative expression HSP12/ALG9
Relative expression HXT7/ALG9
Relative expression MTH1/ALG9
Glucose
16 min no gluc.
32 min no gluc.
WT
pin4Δ
pin4RRMΔ
pin4RRM-M1
C)
No glucose 16 minutes (RT-qPCRs)
HSP12
HXT7
MTH1
Fold change to WT glucose (HSP12/ALG9)
Fold change to WT glucose (HXT7/ALG9)
Fold change to WT glucose (MTH1/ALG9)
WT
pin4Δ
pin4RRMΔ
pin4ΔCT

Figure 6

A)

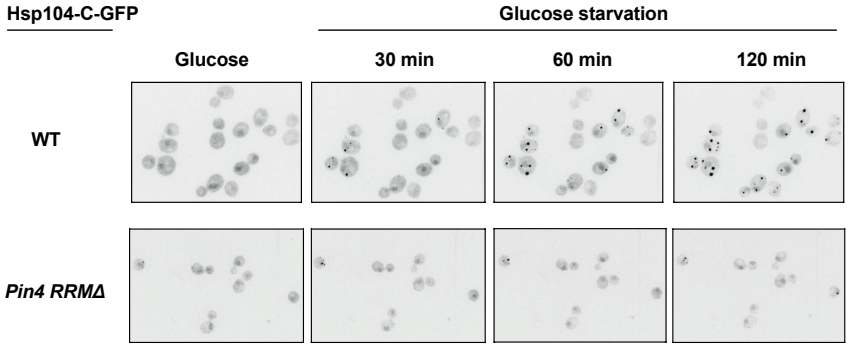
Hsp104-C-GFP
Glucose starvation
Glucose
30 min
60 min
120 min
WT
Pin4 RRMΔ

B)

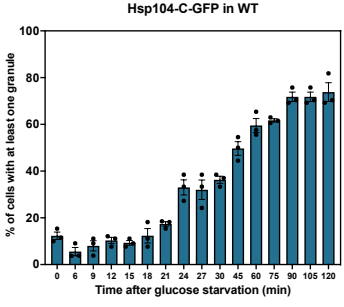
Hsp104-C-GFP in WT
% of cells with at least one granule
Time after glucose starvation (min)

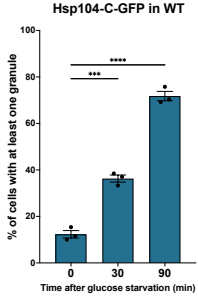
Hsp104-C-GFP in WT
% of cells with at least one granule
Time after glucose starvation (min)

C)

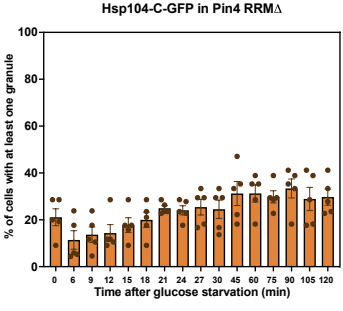
Hsp104-C-GFP in Pin4 RRMΔ
% of cells with at least one granule
Time after glucose starvation (min)

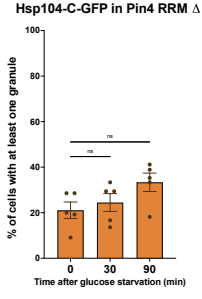
Hsp104-C-GFP in Pin4 RRM Δ
% of cells with at least one granule
Time after glucose starvation (min)

Figure 7

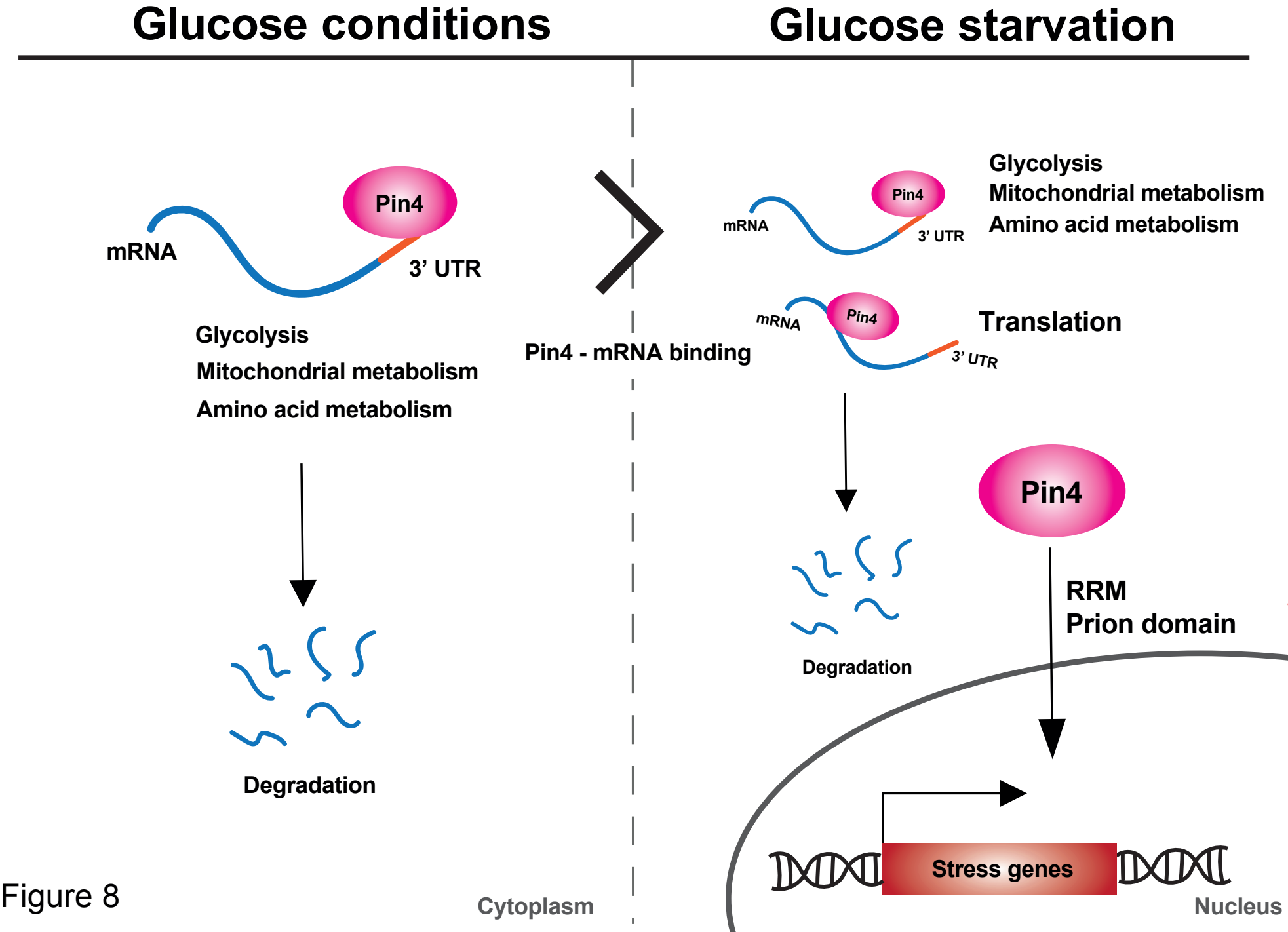
Glucose conditions
Glucose starvation
Pin4
mRNA
3' UTR
Glycolysis
Mitochondrial metabolism
Amino acid metabolism
Degradation
Pin4 - mRNA binding
Pin4
mRNA
3' UTR
Glycolysis
Mitochondrial metabolism
Amino acid metabolism
mRNA
Pin4
3' UTR
Translation
Degradation
Pin4
RRM
Prion domain
Stress genes
Cytoplasm
Nucleus

Figure 8

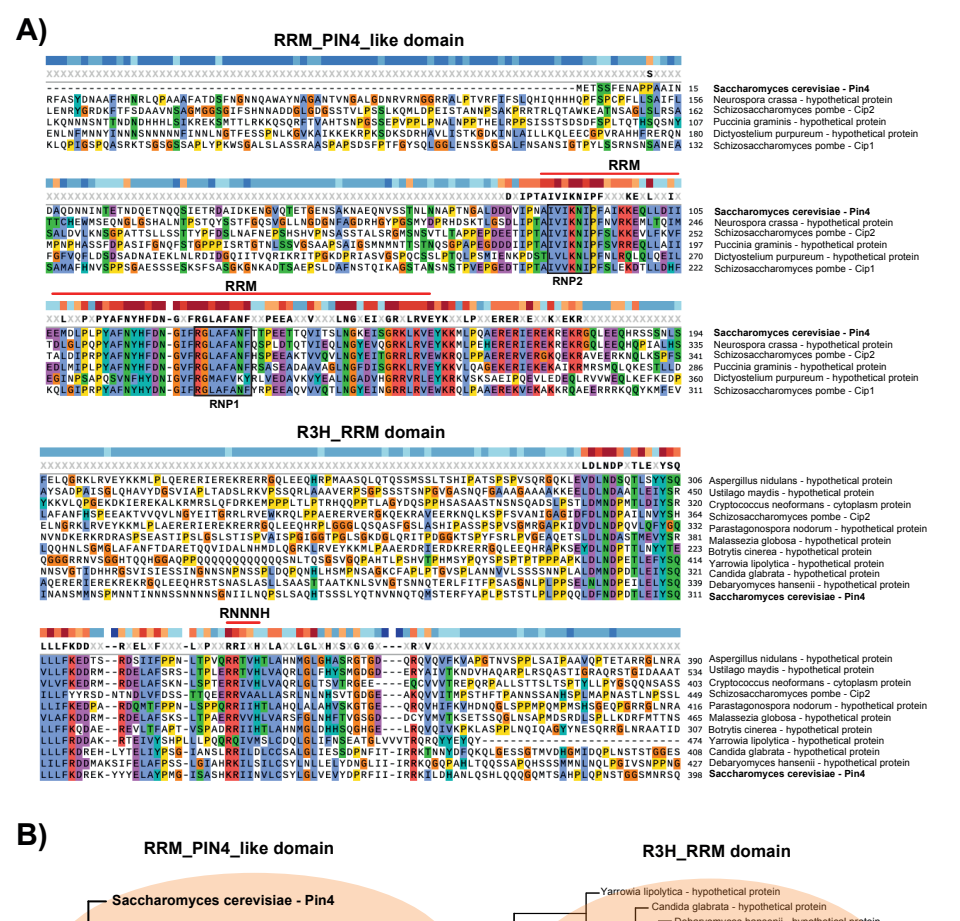

Supplementary Figure 1

A)

Canonical RRM

Position: 3 5

RNP1: (R/K) - G - (**F/Y**) - (G/A) - (**F/Y**) - V - X - (F/Y)

Position: 2

RNP2: (L/I) - (**F/Y**) - (V/I) - X - (N/G) - L

Pin4 RRM

Position: 128 130

Pin4 RNP1: R - G - **L** - A - **F** - A - N - F

Position: 88

Pin4 RNP2: I - **V** - I - K - N - I

B)

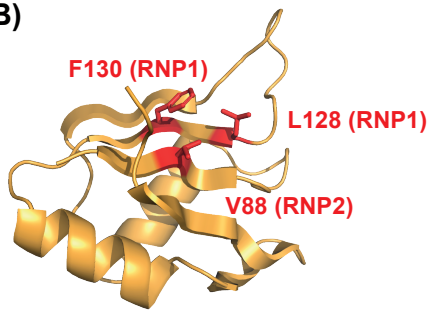

Pin4 RRM

C)

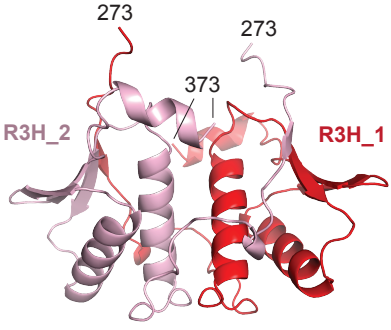

ipTM=0.77 pTM=0.78

D)

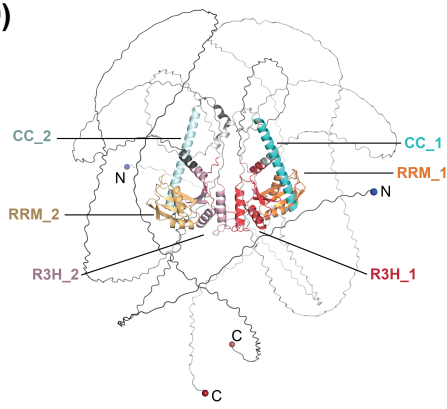

ipTM=0.26 pTM=0.26

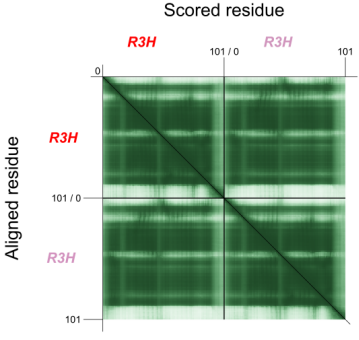

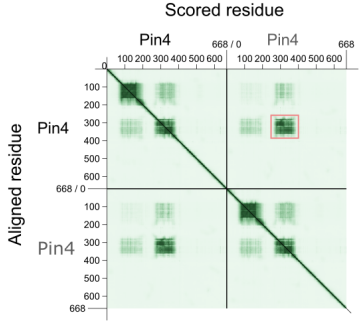

Supplementary Figure 2

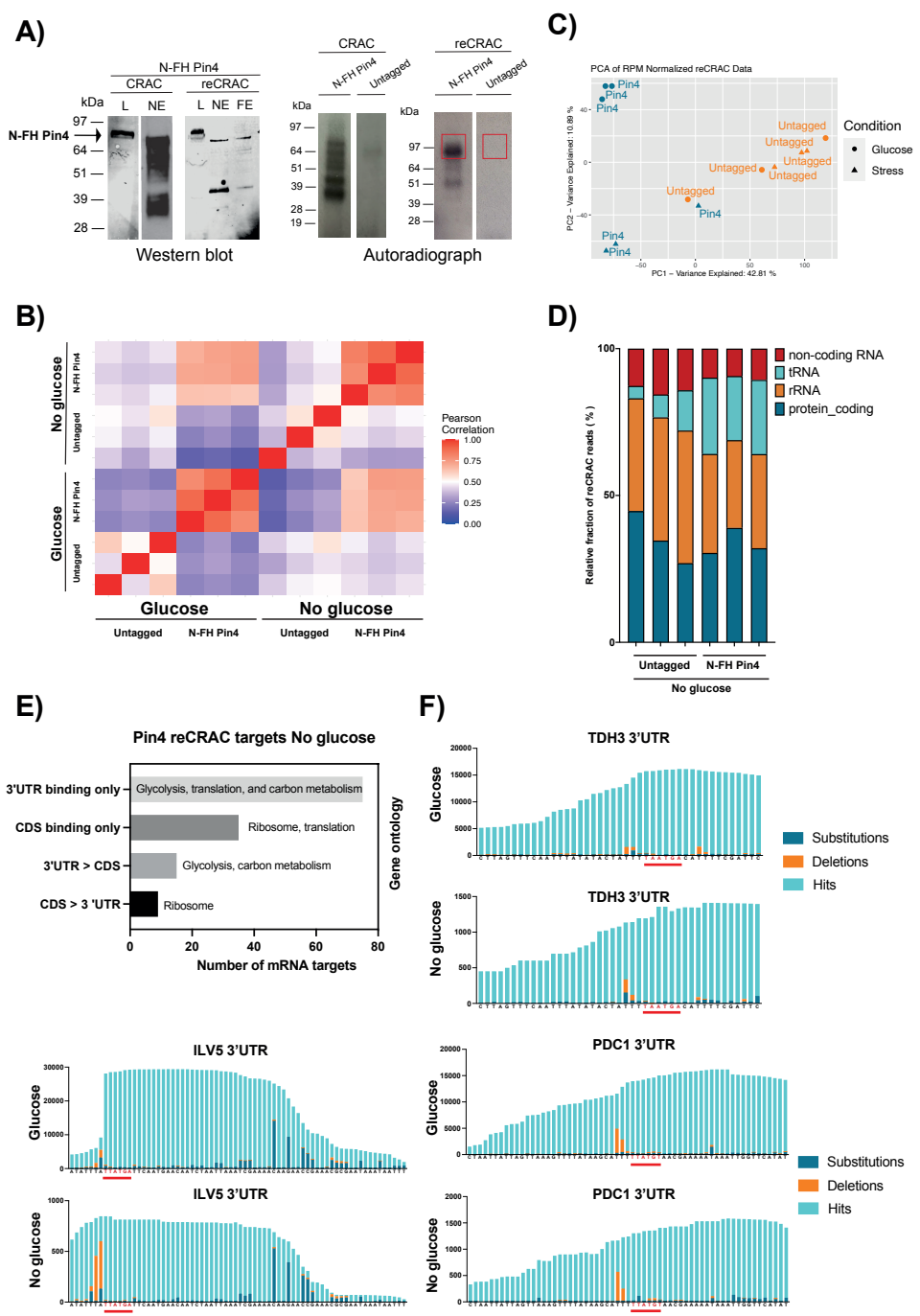

Supplementary Figure 3

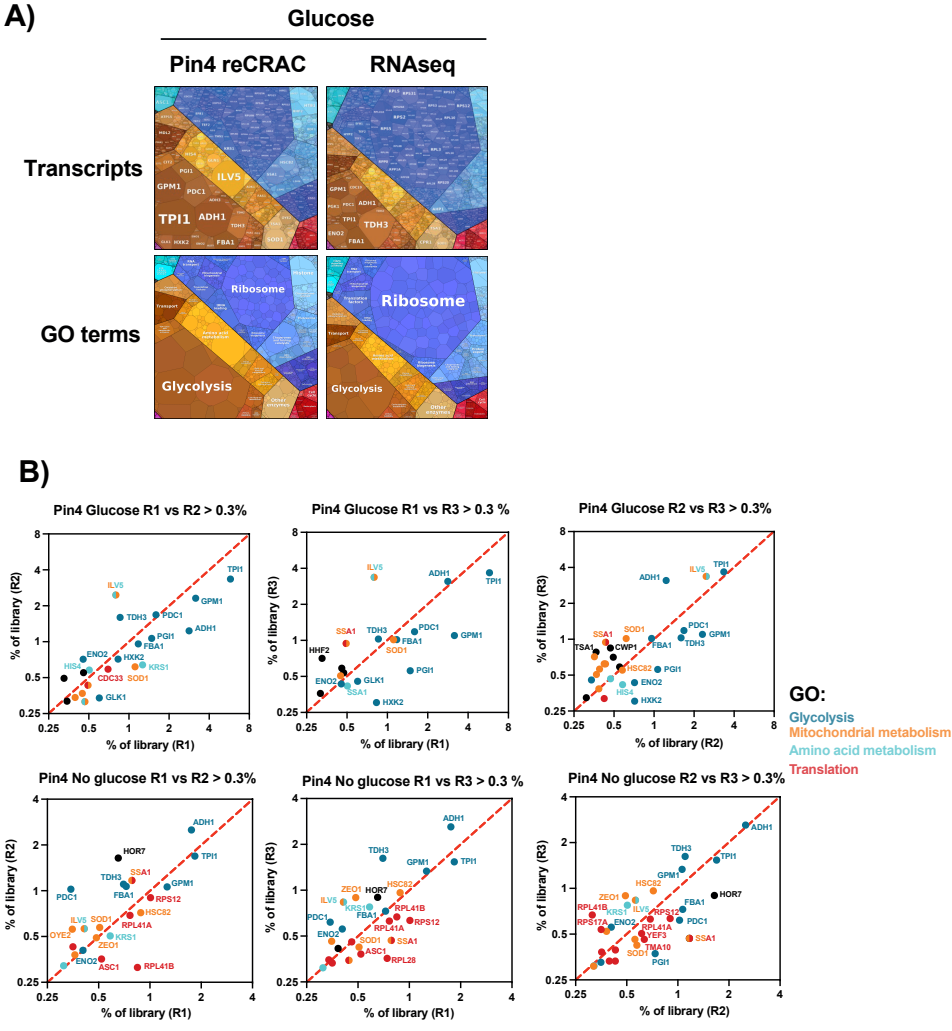

Supplementary Figure 4

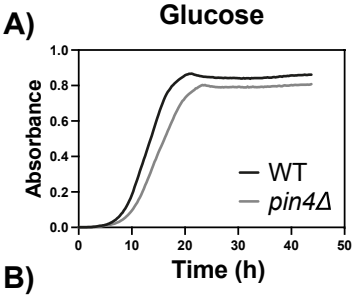

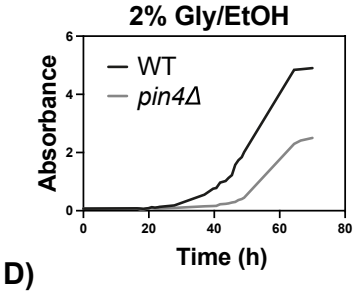

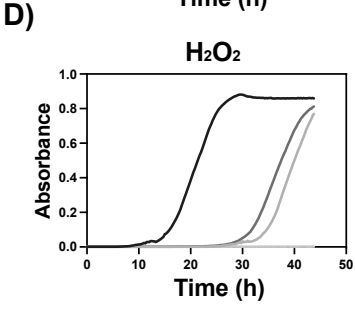

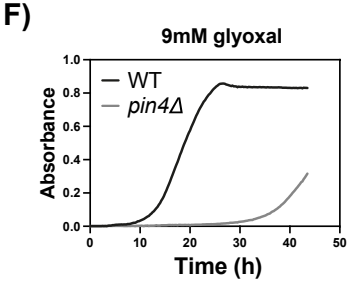

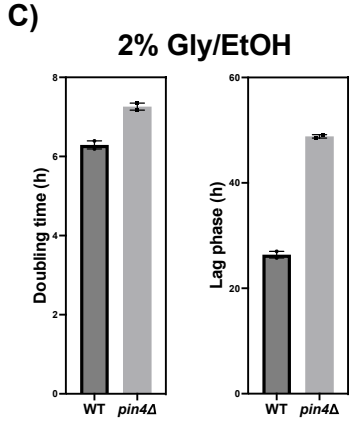

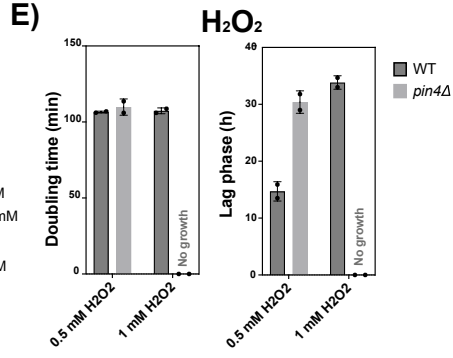

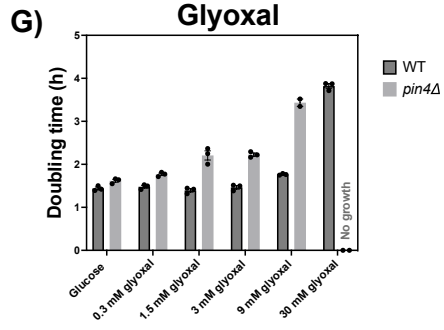

Supplementary Figure 5

A)

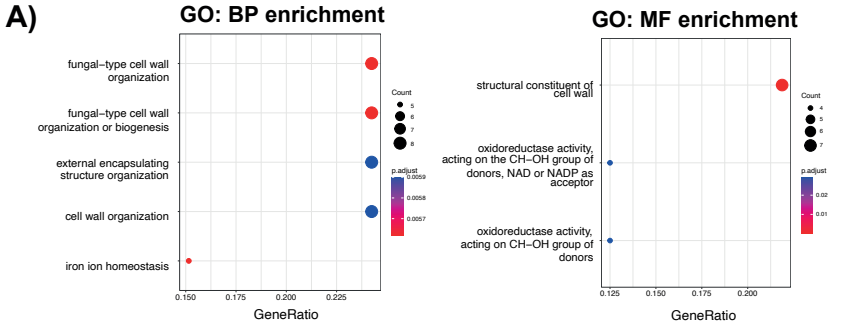

Upregulated in pin4Δ vs WT glucose

B)

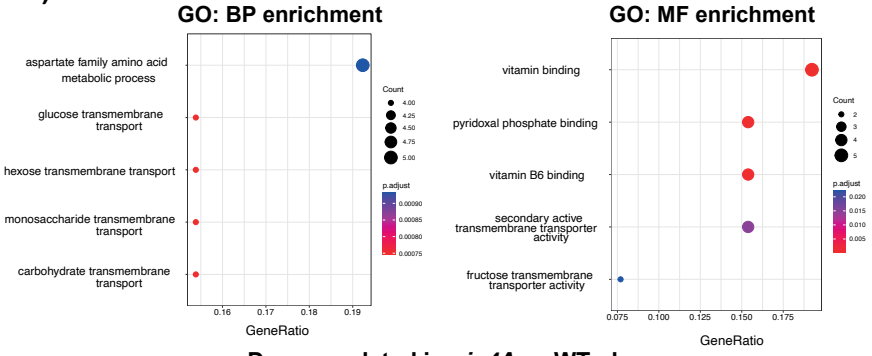

Downregulated in *pin4Δ* vs WT glucose

C)

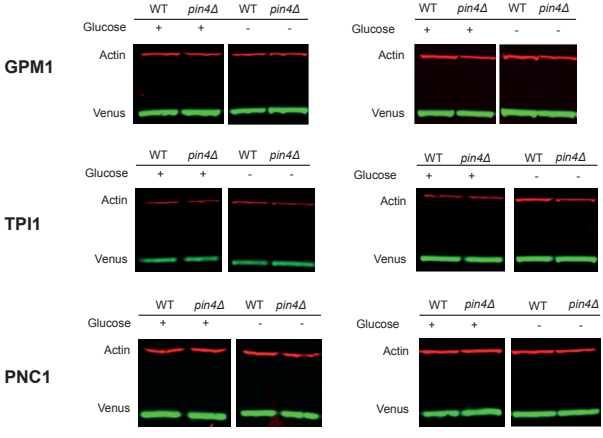

Supplementary Figure 6

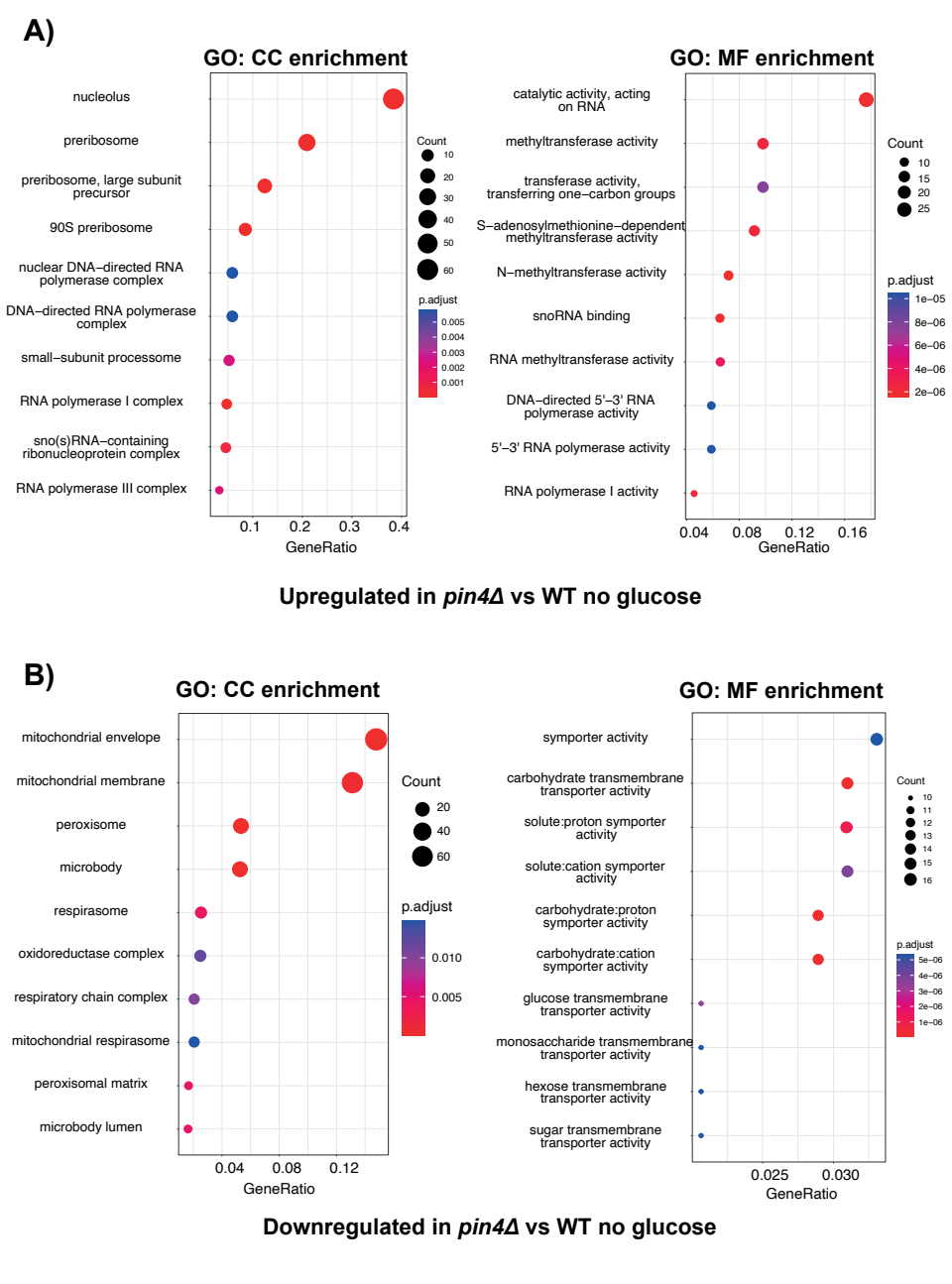

Supplementary Figure 7

Oligo name	Sequence
CRISPR-Cas9	
sgRNA oligos	
#362 N-FH_PIN4_g1	GATCAGGAGCATTCTCAAAAGAACGTTTTAGAGCTAG
#363 N-FH_PIN4_g2	CTAGCTCTAAAACGTTCTTTTGAGAATGCTCC
#491 PIN4_RRM_KO_g1	GATCGTTAGACATTATTGAAGAAAGTTTTAGAGCTAG
#492 PIN4_RRM_KO_g2	CTAGCTCTAAAACTTTCTTCAATAATGTCTAAC
#487 PIN4_RRM_M1_g1	GATCGGTAATTGAAGGCATAAGGAGTTTTAGAGCTAG
#488 PIN4_RRM_M1_g2	CTAGCTCTAAAACTCCTTATGCCTTCAATTAC
oKB080 PIN4_C_terminus_K	GATCTTATTCTCGACTCTAATGAAGTTTTAGAGCTAG
oKB081 PIN4_C_terminus_K	CTAGCTCTAAAACTTCATTAGAGTCGAGAATAA

Repair templates	
#378 N-FH_Pin4_RT1	CAGGCTACAGACTAGGGAAAGCGTGTTCAACAACAATAAGAAATGGATTATAAAGATGACGATGACAAGGCCGCAGCCGCACATC
#379 N-FH_Pin4_RT2	ATCATTGATGGCTGCAGGAGGAGCATTCTCAAAAGAACTAGTCTCGTGATGGTGATGATGGTGGTGATGTGCGGCTGCGGCCTTG
#497 PIN4_RRM_KO_RT1	AAACGTTTCTTCTACAAATTTGAATAATGCCCCCACCAATGGTGCTTTGGACGATGATGTTATCCCAAAT
#498 Pin4_RRM_KO_RT2	CTCGATTCTTTCTCTTTCAGCTTGGGGAAGCATTTTTTTATATTCATTTGGGATAACATCATCGTCCAAA
#493 PIN4_RRM_M1_RT1	CCCAAATGCTATTGCTATTAAAAACATTCCGTTTGCTATTAAAAAAGAGCAATTGTTAGACATTATTGAAGAAATGGATCTTCCTCTTCC
#494 PIN4_RRM_M1_RT2	GGTGAAATTCGCAGCGGCAGCTCCTCTGAAAATACCGTTATCAAAGTGGTAATTGAAGGCATAAGGAAGAGGAAGATCCATTTCTTCAA
oKB082 PIN4_C_terminus_K	GGACAATTAGAAGAACAACACAGATCGTCATCTAATCTTTCTTTGGATTCTTTATCTAAAAGTAAAGGAGAAGAACTTTTC
oKB083 PIN4_C_terminus_K	CGTGCGATATACAAATACCAAACAAACTCTATAATCATAGAATAATGGAAGTATATACTATTTGTATAGTTCATCCATGCC

Supplementary Table 1

Check oligos	
#400 PIN4_N_chk1	GCAGGTCTTTGGAGATTAGCG
#401 PIN4_N_chk2	TCTCACCAGTTTCCGTTTGC
#502 PIN4_RRM_KO_chk1	CGATGACAAGGCCGCAGCCG
#503 PIN4_RRM_KO_chk2	CAAAGAAAGATTAGATGACG
#504 PIN4_RRM_M1_chk1	ACTAATGACCAGGAAACAAA
#500 PIN4_RRM_M1_chk2	GGAAGCATTTTTTTATATTC
oKB084 PIN4_C_terminus_K	CGAGAGGGAGAAGAGAGAGA
oKB061 GFP_tag_reverse	ccgtttcatatgatctgggt
oKB055 PIN4_C_terminus_K	CCAACTGCTTCCACAGCACA
oKB056 PIN4_3UTR_reverse	GCACCCCTCATTACTTGTATCG
oKB57 HSP104_chk1	CCGATGATATGGGTGCACGT
oKB61 HSP104_GFP_revers	CCGTTTCATATGATCTGGGT
oKB058 HSP104_3UTR_reve	GCTCTTTTGCTCGGGTGTCA

PIN4 deletion	
#415 PIN4_KO_1	TACAGACTAGGGAAAGCGTGTTCAACAACAATAAGAAATGcggatccccgggttaattaa
#416 PIN4_KO_2	AACAAACTCTATAATCATAGAATAATGGAAGTATATATTAgaattcgagctcgtttaaac
#413 PIN4_KO_chk1	TTCAGGTTAATGATGGTGTTC
#1 KANMX4_up_2	ATTCTGGGCCTCCATGTCGCTG
#417 PIN4_wt_chk1	CACCTCCAAATTCACAAATC
#418 PIN4_wt_chk2	CGCTTAAAGAACGATTCAAG

GFP tagging	
#551_HSP104_GFP_C_FP	CGTTAGGTGATGACGATAATGAGGACAGTATGGAAATTGATGATGACCTAGATcggatccccgggttaattaa
#552_HSP104_GFP_C_RP	GTTTTATTAATTATATATATTATATTACTGATTCTTGTTCGAAAGTTTTTAAAAATCACACTATATTAAAgaattcgagctcgtttaaac

Reporter constructs	
#526_TPI1_3UTR_FP	GCATCGTCTCATCGGTCTCAATCCTAAGATTAATATAATTATATAAAAATATTATCTTCTTTTCTTTATATCTAGTGTTATGTAAAATAAATTGATGAC
#527_TPI1_3UTR_RP	ATGCCGTCTCAGGTCTCACAGCGCAATATTAAAATATAGAAGCCCAAATTTTATATTTCAAATGAATAAATG

Supplementary Table 1

#528_ GPM1_3UTR_FP	GCATCGTCTCATCGGTCTCAATCCTAAGTCTGAAGAATGAATGATTTGATGATTTCTTTTTCCCTCCATTTTTCTTACTGAATATATCAATGATATAG
#529_ GPM1_3UTR_RP	ATGCCGTCTCAGGTCTCACAGCAATTATCTCAAAATTCACCAACCTCTCATGGCGCATATTCATCATGCATGTAACTACCACATCAATG
#532_ PNC1_3UTR_FP	GCATCGTCTCATCGGTCTCAATCCTAAGAGCTGAATAATACTTCTTCAACCTGATGAACTAGGGTGGCTTGCAAATGCACAAATCTATATAACAATATC
#533_ PNC1_3UTR_RP	ATGCCGTCTCAGGTCTCACAGCCAGATGGGGAGAGAGAATGTGGATTGGCGAGAAATAATGTCGGTATTCGAAGAAGGC
#468_Part_plasmid_chk1	acgccagcaacgcggcctttttacgg
#469_Part_plasmid_chk2	gctcgcttggactcctgttgatagatcc
#540 HO 5' forward	CACATCATTTTCGTGGATCC
#541 HO 5' reverse	ACAGCGATGGAACTTACGGC
#542 HO 3' forward	TATCGTGTTGCATCTGCGGC
#543 HO 3' reverse	CTTTGGACTTAAAATGGCGT

RT-qPCR	
#544_Venus_CDS_forward	TTCACTGGTGTTGTCCCAAT
#555_Venus_CDS_reverse	GGCCATGGAACTGGCAATTTA
#516 MTH1_RT_qPCR_forwa	TACAGTAGCGACCGCTAGAA
#517 MTH1_RT_qPCR_rever	TTCTCCATTCCGGTTTCGAC
#518 HXT7_RT_qPCR_forwa	AACTCCTGTGGAGCATCTCT
#519 HXT7_RT_qPCR_rever	GTGCTCTTCACCTTCACCAT
#520 HSP12_RT_qPCR_forw	AGGCAAGGATAACGCTGAAG
#521 HSP12_RT_qPCR_reve	AACATATTCGACGGCATCGT
#536 ALG9_RT_qPCR_forwa	GAAGCTTGCTCCTGTATCAT
#537 ALG9_RT_qPCR_rever	GCAGTGGGAAATTCAGTAAC

Supplementary Table 1. The list of oligonucleotides used in this study.

Strain Name	Species	Genotype	Resistance
BY4741	S. cerevisiae	MATa his3D1 leu2D0 met15D0 ura3D0	None
N-FH PIN4	S. cerevisiae	MATa his3D1 leu2D0 met15D0 ura3D0 N-FH PIN4	None
pin4Δ	S. cerevisiae	MATa his3D1 leu2D0 met15D0 ura3D0 pin4Δ	None
N-FH Pin4 RRMΔ from A86 to V158	S. cerevisiae	MATa his3D1 leu2D0 met15D0 ura3D0 N-FH Pin4 RRMΔ	None
N-FH Pin4 RRM M1 (V88A, L128A, F130A)	S. cerevisiae	MATa his3D1 leu2D0 met15D0 ura3D0 N-FH Pin4 RRM M1 (V88A, L128A, F130A)	None
Hsp104-GFP-C	S. cerevisiae	MATa his3D1 leu2D0 met15D0 ura3D0 Hsp104-GFP-C	Kan
Hsp104-GFP-C in Pin4 RRMΔ	S. cerevisiae	MATa his3D1 leu2D0 met15D0 ura3D0 Hsp104-GFP-C N-FH Pin4 RRMΔ	Kan
Pin4 C-terminus Δ	S. cerevisiae	MATa his3D1 leu2D0 met15D0 ura3D0 Pin4 C-terminus Δ	None
pTEF2-Venus-TPI1 3'UTR MoClo Reporter in By4741 background	S. cerevisiae	MATa his3D1 leu2D0 met15D0 ura3D0 pTEF2-Venus-TPI1 3'UTR	Hygro
pTEF2-Venus-GPM1 3'UTR MoClo Reporter in By4741 background	S. cerevisiae	MATa his3D1 leu2D0 met15D0 ura3D0 pTEF2-Venus-GPM1 3'UTR	Hygro
pTEF2-Venus-PNC1 3'UTR MoClo Reporter in By4741 background	S. cerevisiae	MATa his3D1 leu2D0 met15D0 ura3D0 pTEF2-Venus-PNC1 3'UTR	Hygro
pTEF2-Venus-TPI1 3'UTR MoClo Reporter in pin4Δ background	S. cerevisiae	MATa his3D1 leu2D0 met15D0 ura3D0 pin4Δ pTEF2-Venus-TPI1 3'UTR	Hygro
pTEF2-Venus-GPM1 3'UTR MoClo Reporter in pin4Δ background	S. cerevisiae	MATa his3D1 leu2D0 met15D0 ura3D0 pin4Δ pTEF2-Venus-GPM1 3'UTR	Hygro
pTEF2-Venus-PNC1 3'UTR MoClo Reporter in pin4Δ background	S. cerevisiae	MATa his3D1 leu2D0 met15D0 ura3D0 pin4Δ pTEF2-Venus-PNC1 3'UTR	Hygro

Supplementary Table 2. The list of strains generated in this study.

Plasmids made in this study	Notes
#1_pML104_N_FH_PIN4	pML104 plasmid containing #362 and #363 sgRNAs
#2_pML104_PIN4_RRM_KO	pML104 plasmid containing #491 and #492 sgRNAs
#3_pML104_PIN4_RRM_M1	pML104 plasmid containing #487 and #488 sgRNAs
#4_pML104_PIN4_C_terminus_KO	pML104 plasmid containing oKB080 and oKB081 sgRNAs
#5_TPI1_Part_plasmid	pYTK001 MoClo plasmid with TPI1 3'UTR sequence = tTPI1
#6_GPM1_Part_plasmid	pYTK001 MoClo plasmid with GPM1 3'UTR sequence = tGPM1
#7_PNC1_Part_plasmid	pYTK001 MoClo plasmid with PNC1 3'UTR sequence = tPNC1

.Supplementary Table 3. The list of plasmids generated in this study.

3'UTR Pin4 binding only No glucose	CDS Pin4 binding only No glucose	Pin4 CDS > 3'UTR binding No glucose	Pin4 3'UTR> CDS binding No glucose
TPI1	FES1	YLR154C-G	ACO1
HOR7	RPL43B	RPS17A	RPL41A
ILV5	YGL088W	RPS12	RPL27A
PGI1	YNL208W	RPL41B	CDC19
OYE2	YDR445C	ZEO1	TEF1
TMA10	ARG82	PGK1	ADH1
RGI1	RPS18B	YEF3	TEF2
ATO3	ACC1	SOD1	FBA1
SSA1	SSU72	RPL9A	PDR16
ALD5	RPS23A		PDC1
HXK2	YKL066W		ENO2
ASC1	RPS9B		TDH3
GLK1	AUR1		GPM1
GLN1	RPS28A		KRS1
PMA1	SAP155		HSC82
RHR2	RPL3		
EFB1	TBS1		
PFK2	RPL15A		
CHO1	FYV1		
RPL20A	RPS17B		
TDH2	RPL42B		
FAS1	RPS23B		
RPL13B	TMA19		
HHF2	RPS6A		
CIT2	RPS3		
HTB1	MTC7		
TAL1	CUP1-2		
BDF1	YPR108W-A		
RPS4A	CUP1-1		
RPS25A	RPL28		
ERG25	RPL23B		
NCE102	RPS6B		
RPL2B	RPS31		
SNX3	RPL10		
LSM6	YDR278C		
HXT3			
ATP15			
RPL42A			
CDC33			
RPS15			
RPS29B			

Supplementary Table 4.

RPS5			
PSA1			
GDH1			
RDL1			
THS1			
ENO1			
RPL22A			
RPS24A			
RPL12A			
RPS1A			
CIT1			
RPL40B			
SED1			
EFT2			
HIS4			
YJL133C-A			
HHT2			
ADK1			
CCW12			
ECM33			
OLE1			
RPL38			
RPS20			
PMT2			
GIS2			
SSB2			
NUS1			
OPI3			
ARF2			
TSA1			
RPS0A			
RPL34A			
OCA1			
RPL35A			

Supplementary Table 4. The list of Pin4 reCRAC 3' UTR and CDS binding mRNA targets following glucose starvation for 16 min.